Coordinated Rho1-dependent mechanical cell-to-cell interactions and medioapical contractile pulsing regulate morphogenesis in the *Drosophila* retina

Christian Rosa Birriel[1], Jacob Malin[1] & Victor Hatini[1*]

[1]Tufts University School of Medicine, Department of Developmental, Molecular & Chemical Biology, Program in Cell, Molecular and Developmental Biology, Program in Genetics, and Program in Pharmacology and Experimental Therapeutics, 150 Harrison Avenue, Boston, MA 02111, United States

*Corresponding author: Victor.Hatini@tufts.edu

ABSTRACT

A striking feature of lattice cells (LCs) in the developing *Drosophila* retina is their constant movement and changes in size and shape before attaining their final form. Previously we showed that repeated contraction and expansion of apical cell contacts contribute to these movements and shape changes. Here we describe a second factor required for these dynamics, the assembly of a medioapical actomyosin ring composed of nodes linked by filaments that attract each other, fuse, and contract the apical cell area of LCs. This medioapical actomyosin network is dependent on Rho1 and its known effectors. Contraction of the apical cell area alternates with relaxation generating pulsatile changes in apical cell area. Strikingly, cycles of contraction and relaxation of cell area within one LC are reciprocally synchronized between adjacent LCs. Further, we identified upstream Rho1 regulators in a genetic screen and found that RhoGEF2 activated these Rho1 functions while RhoGAP71E/C-GAP inhibited them. Thus, Rho1 signaling regulates pulsatile contraction of medioapical actomyosin networks exerting force on neighboring cells, coordinating cell behavior across the epithelium. This ultimately serves to control cell shape and maintain tissue integrity through the process of epithelial morphogenesis of the retina.

INTRODUCTION

A characteristic feature of the developmental elaboration of the *Drosophila* retina is the constant movement of cells entailing changes in cell shape, size, and junctions' length that seem largely transient. Through this process that unfolds over tens of hours, epithelial cells will achieve precise changes in arrangement, cell number, and shape. The result is a tessellated structure composed of approximately 800 nearly identical ommatidia (Cagan and Ready, 1989). This process is a model for understanding epithelial morphogenesis in a fully differentiated tissue forming a mature organ. Each ommatidium consists of four central cone cells, surrounded by two large semi-circular primary (1°) cells. These are surrounded by lattice cells (LCs) and mechanosensory bristles (Fig. 1A). Of these, the LCs exhibit a particularly intricate developmental sequence in which they intercalate with each other to arrange in a single file between ommatidia, extra LCs are pruned, and the remaining cells undergo dramatic shape changes according to their location in the tissue (Cagan, 2009; Carthew, 2007; Johnson, 2021).

The initial arrangement of cells in ommatidia is controlled by differential adhesion (Bao and Cagan, 2005; Bao et al., 2010; Hayashi and Carthew, 2004). After the intercalation of LCs, certain cytoskeletal networks are preferentially associated with a subset of LCs' contacts. Specifically, we showed that contractile junctional actomyosin networks assemble at and contract the LC-LC contacts. These contractile networks are counterbalanced by protrusive branched F-actin networks that assemble along the same contacts with reciprocal dynamics (Del Signore et al., 2018; Malin et al., 2022). This interplay of contractile and protrusive forces along cell edges guides, at least in part, their movements, and prevents errors in the ultimate arrangement and shaping of the cells.

In addition to the junctional cytoskeletal networks, a second actomyosin network called the medioapical actomyosin network is present in the developing fly retina. In 1° cells, this network assembles MyoII foci that correlate with the contraction of cell area. Severing the medioapical actomyosin network in the 1° cells using laser nano-ablation expanded the apical cell perimeter, indicating that the network applies tension on the apical cell surface (Blackie et al., 2020). However,

the role of this network in lattice remodeling, its dynamic properties, and regulation by upstream signals remain unknown. Medioapical actomyosin networks have been observed during epithelial remodeling in several processes in *Drosophila*, including gastrulation, germband extension, and dorsal closure (Azevedo et al., 2011; Blanchard et al., 2010; Fernandez-Gonzalez and Zallen, 2011; Martin et al., 2009; Rauzi et al., 2010). In those systems, the medioapical actomyosin networks pulse, repeatedly assemble and disassemble, and disrupting their pulsatile dynamics affect cell behavior and leads to epithelial remodeling errors. However, these early developmental processes fundamentally differ from the remodeling of the retina. They entail massive reorganization of cells that takes place over the time course of tens of minutes, compared to the precise refinement of the retina, which takes tens of hours. Furthermore, the pulsation typically displays a ratcheting characteristic, where relaxation after constriction is only partial, and the cells never revert to their original shape. In contrast, in the retina, there is no obvious ratcheting characteristic to cell-shape changes.

Cell movement and changes in shape are, however, characteristics of epithelial morphogenesis of the retina (Blackie et al., 2021; Blackie et al., 2020; Del Signore et al., 2018; Johnson et al., 2008; Larson et al., 2008; Letizia et al., 2019; Malin et al., 2022; Seppa et al., 2008). These changes are clearly critical for generating the very precise organization of the retina because errors occur when they are perturbed. Thus, a major challenge is identifying mechanisms that regulate cell dynamics and understanding their impact on force generation, force transmission, and the eventual attainment of specific cell shapes.

Here we used the *Drosophila* LCs to investigate the dynamic properties of the medioapical actomyosin network that support apical epithelial remodeling using high-resolution live imaging and laser nano-ablation combined with genetic tests of gene function. We asked if medioapical actomyosin networks pulse and studied their contribution to cell shape changes. We found a pulsatile medioapical actomyosin network, whose assembly promoted the transient, anisotropic contraction of LCs. Our experiments revealed the interplay between the assembly and disassembly of medioapical

actomyosin networks and mechanical interactions between neighboring cells. In addition, we identified upstream regulators of Rho1, which control the assembly of the medioapical actomyosin network. While some features were reminiscent of other developmental processes involving medioapical actomyosin networks, many aspects are unique to this late-stage developmental process. Overall, our data provide evidence that biochemical and mechanical signals that function to control Rho1 activation are required to rebalance forces in the epithelium, control cell shape and rearrangements, and maintain tissue integrity.

RESULTS

A dynamic medioapical actomyosin network assembles during LCs' remodeling

The developing fly retina is a model for understanding how force-generating cytoskeletal networks control cell shape changes, cell-cell interactions, and tissue patterns (Fig. 1A). During lattice remodeling, the 2° LCs narrow and elongate to form the edges of the lattice while the 3° LCs compact to form alternating corners. To examine the behaviors of the medioapical actomyosin network during lattice remodeling, we live imaged F-actin with the actin-binding domain of Utrophin tagged with GFP (Utr::GFP) together with Spaghetti Squash (Sqh), the regulatory light chain of non-muscle Myosin II (MyoII), tagged with mCherry (MyoII::mCh). We found that F-actin and MyoII accumulated in particles that flowed from the apical cell surface toward the cell's medioapical region, forming a dynamic ring-like structure (Fig. 1B, red arrow). These particles were then remodeled and disassembled (Fig. 1B, green arrows). Time-shifted Pearson correlation analysis confirmed that medioapical F-actin and MyoII accumulated with the same dynamics, suggesting that they co-assemble to form the contractile actomyosin network (Figs. 1B', S1A-B', R= 0.4400). In time-lapse movies, we observed fluctuations in the LCs' apical area (Fig. 1B) and asked if they correlated with fluctuations in actomyosin levels. We found a significant negative correlation between medioapical F-actin and LCs' apical area (Figs. 1B", S1B"). We also observed that medioapical F-actin levels peaked 15-20 sec before maximal cell area contraction (Fig. S1B'', R= -0.2706). These results suggest that the medioapical actomyosin network

exerts tension dynamically on the apical cell perimeter leading to a reduction in the apical cell area upon an increase in actomyosin levels. This observation is consistent with a previous report showing that MyoII accumulation in medioapical foci in the 1° cells correlated with a decrease in the cells' apical area (Blackie et al., 2020).

The Rho1 Rho GTPase controls the contractile actomyosin network assembly and contraction by activating the formin Diaphanous (Dia), which assembles linear F-actin filaments, and Rok, which phosphorylates the MyoII regulatory light chain to activate MyoII (Homem and Peifer, 2008; Magie et al., 1999; Mizuno et al., 1999; Mulinari et al., 2008; Warner and Longmore, 2009a; Warner and Longmore, 2009b). To determine if Rho1 functions medioapically, we examined the accumulation of GFP-tagged Rho1 and Rok reporters relative to F-actin marked with the F-actin-binding peptide Lifeact tagged with the Ruby fluorescent protein (Lifeact::Ruby). We found that both Rho1 and Rok accumulated medioapically in dynamic particles (Fig. 1C and D, yellow arrows). The accumulation of Rho1 and Rok in the medioapical region during LCs' apical remodeling suggested that the two proteins control medioapical actomyosin dynamics.

To better understand how the medioapical actomyosin ring-like structure forms, we imaged the network at a higher temporal resolution, obtaining an image stack every 5 seconds. We found that some F-actin particles moved toward one another during ring formation and merged to form a larger particle (Fig. 1E-E'; Movie 1). As the ring disassembled, some particles disappeared while others flowed toward cell edges and merged with the junctional network (Fig. 1E"; Movie 1). The medioapical ring assembled approximately every 6 min (Fig. 1F; 349 +/- 96 sec), with a 1.4-fold increase in F-actin levels from trough to peak in each cycle (Fig. 1G). This network behavior suggests that medioapical actomyosin forms a network composed of interconnected nodes that pull on one another and the cell surface in a process controlled by Rho1 and Rok.

Medioapical actomyosin exerts tension on the apical cell surface and is mechanically adaptive

Using high-resolution Airyscan confocal imaging, we examined the structure of the medioapical actomyosin network at higher spatial resolution in time-lapse movies. We identified nodes that form the medioapical ring-like structure and filamentous structures between nodes and between nodes and the cell surface (Fig. 2A, left panel, yellow arrows). Some F-actin filaments connected to nodes were linked perpendicularly to LC-LC contacts, which are sites dynamically rich in F-actin (Fig. 2A, right panel, yellow arrows). This architecture suggested that the network exerts tension on the cell surface and that LCs are mechanically linked through a dynamic supracellular medioapical actomyosin network anchored, in part, at the LC-LC contacts.

To study the role of the medioapical actomyosin network in tissue mechanics, we ablated the network either partially or entirely and investigated the cell-autonomous and non-autonomous effects. We first ablated the network in the 2° LCs and found that F-actin structures recoiled toward the cell periphery (Fig. 2B, flow marked by an ellipse, LC-LC contacts with a white arrow). Concomitantly, we observed a rapid non-isometric relaxation of the apical cell area preferentially parallel to LC-LC contacts (Fig. 2B, C, Movie 2). The severing and recoil of the medioapical actomyosin network resulted increased the 2° LCs' total area by an average of 2-fold, resulting from a 2-fold cell area expansion along the shorter axis, while the longer axis was not significantly affected (Fig. 2B- C, E). We next ablated the 3° LCs and observed a similar 2-fold increase in the apical cell area (Fig. 2D-E, Movie 2). Additionally, we found that both the 3°-2° and 3°-1° contacts expanded, though 3°-1° contacts expanded more than 3°-2° contacts (Fig. 2E). These mechanical responses suggest that the medioapical actomyosin network contracts the apical cell area asymmetrically to preferentially shrink the LC-LC and 3°-1° contacts and guide the eventual shape changes of the LCs. Overall, the recoil patterns of the apical cell area of 2° and 3° LCs suggest that in 2° LCs, the medioapical actomyosin network promotes the shortening of LC-LC contacts, while in 3° LCs, it preferentially shortens the 3°-1° contact and contributes to the shortening of 3°-2° contacts (see model in Fig. 2F).

The ablation of a 2° LC expanded the LC-LC contact and thus affected the adjacent non-ablated LC by stretching their shared contact. We observed that in response to this stretch, the neighboring non-ablated LC assembled a medioapical actomyosin network to contract its apical cell area and shorten the LC-LC contact (Fig. 2G). This mechanical response implies that the LCs sense their mechanical state and adapt to restore proper intercellular force balance.

Rho1 regulates the frequency and amplitude of medioapical actomyosin network assembly

We next investigated mechanisms affecting the assembly of the medioapical actomyosin network during LCs' remodeling. The Rho1 Rho GTPase activates effectors that promote the assembly and contractility of actomyosin networks (Ridley and Hall, 1992). Therefore, we hypothesized that the Rho GTPase cycle controls medioapical actomyosin network assembly and disassembly and, thereby, the observed fluctuations in apical cell area. To test the role of Rho1 and actomyosin dynamics in eye epithelial remodeling, we first manipulated Rho1 function itself. We reasoned that inhibiting or activating Rho1 would impair these dynamics and reveal their role in lattice remodeling. To test whether Rho1 affected medioapical actomyosin dynamics, we first expressed a dominant-negative Rho1 ($Rho1^{DN}$) and investigated the impact on medioapical F-actin dynamics. We found a general increase in apical cell areas and large fluctuations in cell area over time (Fig. 3A, yellow arrows mark LC-LC contacts). While both the junctional and medioapical F-actin were sparse, as expected, cell area fluctuations were still observed, and contractions were accompanied by the assembly of a medioapical actomyosin network that appeared to exert tension and contract the cell surface, thus preventing cells' overexpansion (Fig. 3A, red arrows). Thus, despite the impairment in F-actin levels and organization, LCs were still able to sense their expanded state and adapt by assembling a medioapical actomyosin network to contract the apical cell area.

To test whether Rho1 was sufficient to affect medioapical actomyosin dynamics, we conditionally overexpressed WT Rho1 using the $GAL4/GAL80^{ts}$ system. By conditionally expressing Rho1, we maintained proper tissue integrity and cell connectivity in the epithelium in these eyes. Rho1

overexpression promoted the fusion and enlargement of the medioapical F-actin nodes (Fig. 3B, Movie 3). This was accompanied by an increased pulse frequency (245 +/- 50 sec in Fig. 3C', compared with the 349 +/- 96 sec in WT in Fig. 1F) and an F-actin pulse amplitude of 4.5-fold change (Fig. C", compared with 1.4-fold change in WT in Fig. 1G). While peak medioapical F-actin correlation with cell area contraction in WT was modest (Fig. 1B", R= -0.2706 at -15 sec), LCs overexpressing Rho1 showed a stronger time correlation between F-actin enrichment and cell area contraction (Fig. 3C''' and D, R= -0.6508 at -15 sec). These results indicate that Rho1 activity must be tightly regulated to control the amplitude and frequency of medioapical actomyosin assembly and activation.

Rho1 overexpression reveals cell-to-cell mechanical interactions

The strong fluctuations in apical cell area and medioapical actomyosin assembly induced by Rho1 overexpression prompted us to ask whether nearby cells coordinate their mechanical behavior. We focused on the behavior of adjacent 2° LCs prior to the completion of cell pruning. In this cell configuration, one LC shares only one contact with the neighboring LC and a second with a mechanosensory bristle, while the second LC shares a second contact with a flanking 3° cell. Thus, adjacent LCs are exposed to the minimum of possible mechanical inputs from neighboring LCs, allowing us to isolate the mechanical interactions between these cells with low "background interference" from other neighboring cells. Inspection of time-lapse movies revealed that a contraction of a 2° LC induced a two-step response in the adjacent 2° cell (Movie 4). In the first step, the second 2° LC disassembled its medioapical actomyosin network and its apical area expanded (Fig. 3E at 210 sec, green arrow). In the second step, the second 2° LC reassembled its medioapical network and contracted its apical cell area (Fig. 3E at 595 sec, red arrow). In turn, the contraction of the second 2° LC induced the same two-step response in the first 2° LC. These cell-to-cell mechanical interactions resulted in frequent inversely coordinated cycles of expansion and contraction in adjacent LCs. The peak expansion of a LC occurred 15 sec after the maximal contraction of the adjacent LC (Fig. 3E', R= -0.2020). Thus, as one cell contracted, the other expanded, and vice versa (Fig. 3F; Movie 4). We also

observed inversely coordinated cycles of expansion and contraction between adjacent anterior and posterior cone cells and 1° cells (Fig. S2A-B' and C-D, respectively). Thus, the medioapical actomyosin network not only contributes to the constriction of individual LCs' apices but also by exerting force on adjacent LCs that sets up anticorrelated cycles of constriction and relaxation in adjacent cells.

Dynamic activation of MyoII and F-actin is required for tissue integrity and remodeling

Our findings suggested that tissue remodeling requires a pulsatile medioapical network controlled by Rho1 (Fig. 4A). To address this directly, we tested if MyoII and F-actin dynamics contributed to proper remodeling. To investigate the role of MyoII dynamics in this process, we expressed a constitutively active myosin light chain kinase ($MLCK^{CA}$), which constitutively activates MyoII, and examined cellular and cytoskeletal behaviors in these eyes compared with WT. Forces generated by the cytoskeleton are transmitted between cells via bicellular and tricellular adherens junctions (bAJs and tAJs, respectively). To determine the effects of constitutive MyoII activation on cell adhesion, we examined the adherens junctions (AJs) in eyes that conditionally expressed $MLCK^{CA}$ using the $GAL4/GAL80^{ts}$ system. We live imaged α-Catenin tagged with GFP (α-Cat::GFP) to highlight the AJs and found that they were fragmented compared with WT (Fig. 4B-C). A subset of the LCs failed to intercalate and clustered around mechanosensory bristles (Fig. 4C, yellow arrow). We also observed cells that dramatically expanded their apical area, suggesting that they failed to hold tension exerted by the medioapical actomyosin network and were therefore pulled by their neighbors, thus compromising tissue integrity (Fig. 4C, dotted lines). $MLCK^{CA}$ expression decreased cells' apical area (Fig. 4E). Live imaging with MyoII::mCh showed a high level of MyoII across the entire cell perimeter with enhanced accumulation at LC-LC contacts. Additionally, MyoII enriched in a medioapical ring that formed and disappeared repeatedly (Fig. 4F, Movie 5). This medioapical actomyosin ring pulsed on average every 10 minutes (Fig. 4F'), and its assembly correlated with cell area contraction (Fig. 4F'', R= -0.2126). The defects that arise from $MLCK^{CA}$ expression leading to constitutive MyoII phosphorylation imply that dynamic MyoII phosphorylation is required for the spatiotemporal control

of actomyosin assembly, accurate morphogenesis, and the preservation of epithelial integrity. This is consistent with the role of MyoII phosphorylation in other systems (Jordan and Karess, 1997; Kasza et al., 2014; Vasquez et al., 2014).

To determine if F-actin dynamics are also required for eye epithelial remodeling, we expressed a constitutively active form of Dia (Dia^{CA}), which assembles linear actin filaments downstream of Rho1 and examined the resulting phenotypes. We expressed Dia^{CA} conditionally using the GAL4/$GAL80^{ts}$ system. First, we fixed Dia^{CA}-expressing eyes and stained them for E-cad to examine the effects on epithelial organization. We found that Dia^{CA} expression severely affected cell shape and arrangement in ommatidia, resulting in ommatidia with five or even four sides compared to six in WT (Fig. 4D). We also observed intercalation defects and cavitation of cone cells similar to those observed in eyes expressing $MLCK^{CA}$ (Fig. 4C-D, white arrows). Unlike the contraction of LCs in $MLCK^{CA}$ eyes, Dia^{CA} expression significantly increased cells' apical area (Fig. 4E). To determine if Dia^{CA} affects the actomyosin network, we analyzed medioapical F-actin organization and behavior in these eyes (Fig. 4G, Movie 5). In WT, F-actin is enriched both medioapically and at the LC-LC contacts, while in Dia^{CA} expressing eyes, it accumulated uniformly in a thick band at the cell periphery. We also failed to observe medioapical actomyosin ring assembly in LCs that overexpress Dia^{CA}. By binding efficiently to Rho1 through its RhoGTPase-binding domain, Dia^{CA} could inhibit Rok activation and MyoII phosphorylation, and thus the assembly of a contractile medioapical actomyosin network. Overall, these observations imply that medioapical F-actin and MyoII mechanical dynamics maintain a proper force balance in the epithelium, preserving the overall shapes and arrangements of the cells. This further suggests not only that Rho1 activity and levels must be carefully controlled, but also that a balance of assembly and disassembly of the medioapical network is required to achieve tissue stability and promote epithelial remodeling.

RhoGEF2 and RhoGAP71E control medioapical actomyosin dynamics

We hypothesized that Rho guanine nucleotide exchange factors (RhoGEFs) and Rho GTPase activating proteins (RhoGAPs) for Rho1, which respectively activate and deactivate it, could regulate Rho1 medioapical dynamics (Etienne-Manneville and Hall, 2002; Jaffe and Hall, 2005). To identify these putative regulators, we carried out an RNAi screen for RhoGEFs and GAPs that influence eye epithelial remodeling. We also used mutant alleles for a subset of these genes and generated mutant eyes in an otherwise heterozygous background using the Eyeless-GAL4/UAS-Flp (EGUF) technique or patches of mutant cells using the Flp/Frt technique to interrogate the function of these genes. In the EGUF technique, mutant cells that are generated specifically in the eye can rescue the eye from Hid-mediated apoptosis (Stowers and Schwarz, 1999). In this screen, we identified *RhoGEF2* and *RhoGAP71E* based on epithelial remodeling defects in mutant eyes and clones. This led us to hypothesize that both activation of Rho1 by RhoGEF2 and inhibition by RhoGAP71E regulate Rho1's GTPase cycle and drive medioapical pulsatile dynamics during remodeling. We tested these ideas below.

RhoGEF2 accelerates the frequency and amplitude of medioapical actomyosin assembly and cell area fluctuations

To determine the site of RhoGEF2 action, we examined RhoGEF2 localization using a RhoGEF2 reporter tagged with GFP (RhoGEF2::GFP) and marked cell outlines using F-actin with Lifeact::Ruby. RhoGEF2::GFP accumulated medioapically in pulses (Fig. 5A, yellow arrows) that partially overlapped with medioapical F-actin. To determine if RhoGEF2 levels correlate with LCs' area, we measured the correlation between RhoGEF2 levels and cell area over time. We found a weak negative correlation between RhoGEF2::GFP and LCs' area (Fig. 5A', left panel), with peak enrichment of RhoGEF2 occurring 15-20 seconds after peak LC contraction (Fig. 5A', right panel, R= -0.1361).

To test if RhoGEF2 controls medioapical actomyosin dynamics, we examined F-actin and MyoII dynamics in *RhoGEF2* mutant clones and RhoGEF2RNAi-expressing clones. We first examined

MyoII::GFP in *RhoGEF2* mutant clones compared with the nearby WT cells (Fig. 5B, region inside the yellow dotted line). We found that the *RhoGEF2* mutant clone area had severe patterning defects reflected in the number, shape, and arrangement of LCs compared with patches of WT cells (outside the dotted lines). We also found that the 2° mutant LCs could not engage efficiently in medioapical actomyosin contraction (Fig. 5C), which resulted in a lower negative correlation between MyoII accumulation and apical cell area contraction (Fig. 5C', R= -0.195). The RhoGEF2 clonal phenotypes were severe, so we also examined weaker phenotypes in cell clones depleted for RhoGEF2 function by RNAi (Fig. 5D-D", Movie 6). We found a decrease in medioapical actomyosin levels in FLP-Out clones expressing RhoGEF2 RNAi (Fig. 5D'', Movie 6) compared with WT cells (Fig. 5D"). Time-shifted cross-correlation showed a weaker peak correlation (at -15 sec) between MyoII accumulation and apical cell area contraction in clones of LCs that express RhoGEF2 RNAi compared with WT LCs (Fig. 5D"'). These results provide evidence that RhoGEF2 controls the assembly of the contractile medioapical actomyosin network either directly, by regulating Rho1, or indirectly.

We also investigated the impact of RhoGEF2 overexpression on these dynamics. We found that RhoGEF2 overexpression induced robust and frequent fluctuations of the medioapical actomyosin network that coincided with changes in the cell apical area (Fig. 5E, Movie 6). The actomyosin network assembled to form a dense network that correlated with apical area contraction (red arrow) and then disassembled (green arrow), resulting in apical area relaxation. Time-shifted correlation demonstrated that the assembly of the medioapical actomyosin network strongly correlated with the apical cell area contraction (Fig. 5E', R= -0.3688). While in WT, medioapical F-actin levels inversely correlate with cell area 15-20 sec later (Fig. 1B", Fig. S1B'', R= -0.2706), overexpression of RhoGEF2 enhanced this negative correlation (Fig. 5F, R= -0.4076). Furthermore, overexpression of RhoGEF2 accelerated F-actin pulsing frequency (Fig. 5E'', 215 +/- 56 sec) compared with WT (Fig. 5G, 349 +/-96 sec), and enhanced the amplitude of F-actin accumulation during pulsing (Fig. 5E"') compared with WT (Fig. 5H). Thus, RhoGEF2 expression increased the amplitude and frequency of medioapical actomyosin assembly and phenocopied the Rho1 expression phenotypes. The results

suggest that RhoGEF2 activates Rho1 to promote the assembly of a contractile medioapical actomyosin network during LCs remodeling.

RhoGAP71E promotes the disassembly of the medioapical actomyosin network

To determine where in the cell RhoGAP71E acts, we employed a RhoGAP71E reporter tagged with GFP (RhoGAP71E::GFP). Live imaging showed that RhoGAP71E::GFP was enriched along cell-cell contacts and accumulated medioapically during cell area contractions (Fig. 6A, yellow arrow). RhoGAP71E peak correlation occurred 10 seconds after peak LC contraction and levels decreased during apical area expansion (Fig. 6A', R= -0.1399).

To determine if RhoGAP71E controls medioapical actomyosin dynamics, we first examined the effects of *RhoGAP71E* loss on LCs' remodeling. Eliminating *RhoGAP71E* function or expressing RhoGAP71E RNAi in whole eyes produced flies without eyes. However, using the Flp/Frt technique, we were able to recover sparse *RhoGAP71E* mutant cells (Fig. 6B). The *RhoGAP71E* 1° and 2° mutant cells (yellow arrowhead and arrow, respectively) had smaller apical areas compared with WT counterparts (white arrow and arrowhead, Fig. 6B'). This observation suggested that actomyosin assembly and tension exerted on the apical cell membrane were higher in the *RhoGAP71E* mutant cells leading to apical area contraction. To confirm this result, we examined levels of the phosphorylated activated form of MyoII (p-MyoII) in clones expressing RhoGAP71E RNAi and thus depleted for RhoGAP71E function (Fig. 6C). We found an increase in p-MyoII levels in the clones (Fig. 6C') compared with WT cells (Fig. 6C" and C'"). We also live imaged clones expressing RhoGAP71E RNAi (Fig. 6D, Movie 7). Opposite to the effect of *RhoGEF2* loss on cell shape, we found a decrease in the apical cell area in cell clones expressing RhoGAP71E RNAi (Fig 6D') compared with WT cells (Fig. 6D''). The increased assembly of the medioapical actomyosin network in the RhoGAP71E RNAi expressing cells strengthened the negative correlation between MyoII and cell area (Fig. 6D'''). The enhanced assembly of medioapical actomyosin network in the clone's cells also led to an increase in MyoII pulse frequency (212 +/- 69 sec) compared with WT (Fig. 6D''', 387 +/- 177 sec). These results

suggest that RhoGAP71E inhibits medioapical actomyosin network assembly during LCs remodeling, as decreasing RhoGPA71E levels increased the amplitude and frequency of medioapical MyoII assembly.

We also examined the effects of RhoGAP71E overexpression on the medioapical actomyosin and apical cell area fluctuations. RhoGAP71E overexpression expanded the apical cell area and compromised the ability of a subset of cells to hold tension resulting in their dramatic expansion (Fig. 6E-F', yellow arrow). We also observed a loss of continuity of the AJs marked with α-Cat::GFP (Fig. 6F, yellow arrowhead). These results imply that RhoGAP71E overexpression reduced medioapical tension, allowing the apical cell perimeter to relax (Fig. 6F). Although medioapical F-actin fluctuated in these eyes (Fig. 6G, yellow and white arrows, Movie 7), it appeared to be less robust, and network assembly did not correlate with cell area contraction as in WT eyes (Fig. 6G'). Finally, we examined the interaction between RhoGAP71E and RhoGEF2 by co-expressing the two proteins in the retina. While RhoGAP71E expression alone expanded the apical cell area and led to cell intercalation defects, the expression of RhoGEF2 with RhoGAP71E suppressed these phenotypes (Fig. S3A-D). Taken together, these findings show that RhoGAP71E modulates medioapical actomyosin dynamics and tension by inhibiting Rho1 activity medioapically and antagonizing RhoGEF2 function. Thus, RhoGAP71 and RhoGEF2 regulate the Rho1 GTPase cycle and the overall levels of Rho1 activity to control medioapical actomyosin assembly and contractility, which govern cell shape and rearrangements of cell-cell contact.

DISCUSSION

During epithelial remodeling of the fly retina, at least two dynamic actomyosin networks operate at the apical region of the cells. The first is a junctional network that cyclically contracts and expands the LC-LC contacts (Del Signore et al., 2018; Malin et al., 2022). Here we describe the second mechanism essential for accurate morphogenesis: a non-ratcheting pulsatile actomyosin network controlled by Rho1 and its effectors Dia and MyoII. This network is established by flows of F-actin from

the cell surface toward the medioapical region, where it assembles into actomyosin nodes that generate anisotropic contractile force with the highest force predicting the cell edges that will eventually shorten. This force is transient, and upon release, the actomyosin nodes remodel, disassemble or merge with the junctional network. Strikingly, pulses of medioapical contraction and release are reciprocally synchronized between adjacent 2° LCs, revealing that these Rho1-regulated networks are integral to biomechanical feedback coupling. That is, they appear to trigger, and be triggered, by forces between neighboring cells and coordinate their activity. Furthermore, we found that Rho1 activity is positively regulated by RhoGEF2 and negatively by RhoGAP71E. These observations expand our understanding of the role of these players, from their role in early undifferentiated tissue development to a fully differentiated tissue where they work over different time scales and levels of cellular shape determination.

While a previous study reported the existence of medioapical actomyosin networks in the retina with force-generating capacity in 1° cells, our results add significant color to the nature of these networks (Blackie et al., 2020). We show that medioapical actomyosin networks depend on Rho1 and Rho1 effectors Dia and MyoII. Perturbation of these networks not only led to remodeling errors but also to tissue rupture. These findings indicate a crucial role in the mechanical system that promotes epithelial integrity. In contrast to retina 1° cells, we find that the force generated by the actomyosin network in 2° cells is not isometric. When ablated, the largest recoil occurs parallel to LC-LC contacts predicting the edge that will eventually shorten. This is consistent with our previous observation that single *myoII* mutant LCs change shape non-isometrically (Del Signore et al., 2018).

Live imaging of the LCs also revealed the assembly of a medioapical actomyosin ring structure and its dynamics. In many other cases, the medioapical actomyosin network has a morphology referred to as a 'meshwork' (Chanet et al., 2017; Christodoulou and Skourides, 2015; Collinet et al., 2015; He et al., 2010; Maitre et al., 2015; Martin et al., 2009; Rauzi et al., 2010; Solon et al., 2009; Yu and Fernandez-Gonzalez, 2016). This is the case in gastrulation, where cells' resistance to cell contraction is low in one direction and high in the orthogonal direction (Martin et al., 2010). In

experimentally generated round embryos, when the resistant forces are increasingly isometric, the medioapical actomyosin meshwork converts to rings (Chanet et al., 2017). Therefore, it has been postulated that isometric resistance fosters ring formation of medioapical actomyosin networks while directional resistance fosters an apparent meshwork. Taken together with the current observations, a ring structure may be associated with conditions where opposing forces are generally isometric; however, this organization is, in turn, capable of generating asymmetric force.

Our results also revealed the pulsing features of medioapical actomyosin networks in the retina. We found that Rho1 overexpression increased the amplitude of peak F-actin accumulation, peak area constriction, and frequency of apical constriction. This observation suggests that simply the level of Rho1 affects the kinetics of pulsing. However, we found that these characteristics of pulsing had no obvious impact on the persistence of constriction or the appearance of ratcheting. This is different from other systems describing medioapical actomyosin pulsing. For example, in ventral furrow formation, there are correlations between myosin accumulation, the strength of constriction, and the frequency of pulse cycles, but these are, in turn, correlated with the likelihood of ratcheting (Chanet et al., 2017). Thus, our results show unique features of medioapical actomyosin pulsing that depend on the specific developmental process and eventual shape-change required.

Overexpressing Rho1 also dramatically revealed that the rapid cell area oscillations induced were inversely coordinated in adjacent 2° LCs: one cell contracted then relaxed while its neighbor relaxed and then contracted. Although it is known that cells can sense and adapt to mechanical forces (del Rio et al., 2009; Gaertner et al., 2022; Mueller et al., 2017; Spadaro et al., 2017; Yonemura et al., 2010), and medioapical actomyosin generates tension in the retina (Blackie et al., 2020), the current observations expand our understanding of how forces work in this system. The data suggest that neighboring LCs and the medioapical actomyosin networks do not merely strike a balance of mechanical forces but are continually adapting to changing forces over time, generating pulsing changes in cell shape that are coordinated. More specifically, our findings provide evidence that mechanical cell-to-cell interactions can activate or inhibit Rho1 function and actomyosin assembly and

that cells respond to pull and stretch under normal physiological conditions by modulating Rho1 function. Thus, Rho1-dependent medioapical actomyosin networks appear integral to feedback loops that coordinate pulsing between adjacent cells.

Not only was anti-correlated pulsing between adjacent cells detected with Rho1 overexpression, it was also apparent in WT eyes. However, the strength of the correlation between actomyosin accumulation and cell area contraction in WT cells had a wide distribution (Fig. S1B”). This suggests that the pulsing is highly tuned to work in balance with other ongoing cellular processes that may provide permissive conditions, such as the net force exerted by neighboring cells. The anti-correlation of neighboring 2° LCs is a unique feature contrasting with other examples of pulsing contraction. For example, in cell intercalation during germband extension, adjacent cells constrict simultaneously, resulting in loss of contacts and rearrangement of the epithelium (Fernandez-Gonzalez and Zallen, 2011; Rauzi et al., 2010; Sawyer et al., 2011; Vanderleest et al., 2018). In apical constriction, it has been observed that when one cell exhibited ratcheting contraction, ratcheting of nearby cells became more likely, to stabilize changes in cell shape and facilitate invagination (Xie and Martin, 2015). These findings suggest that although Rho1-regulated medioapical actomyosin constriction generally appears sensitive to forces exerted across the epithelium, the cell’s specific response to forces imposed by neighbors is a control point with a variable outcome.

Together, these findings indicate that Rho1 dynamics must be tightly controlled in space and time to regulate actomyosin dynamics and epithelial morphogenesis. Using a genetic screen, we identified RhoGEF2 and RhoGAP71E as upstream regulators of Rho1 and whose perturbation yielded altered cell shape while the integrity of the adherens junctions was maintained. Although we previously identified these genes in a screen for epithelial folding in leg joint morphogenesis, and they are both known regulators of Rho1 in other systems, we were surprised to identify these genes because the characteristics of the medioapical actomyosin network in the LCs are unique (Azevedo et al., 2011; Denk-Lobnig et al., 2021; Fox and Peifer, 2007; Greenberg and Hatini, 2011; Hacker and Perrimon, 1998; Mason et al., 2016; Mulinari et al., 2008). In these other cases involving RhoGEF2 and

RhoGAP71E, there is typically ratcheting shape change, irreversible loss of contacts, and/or epithelial folding, none of which characterize changes in the retina at this phase of development. Thus, identifying RhoGEF2 and RhoGAP71E in this study is important because it reveals that their participation is not linked to a particular morphological outcome. Since pulsing appears regulated by forces imposed by neighboring cells, our results also suggest the hypothesis that mechanical forces could, in turn, regulate RhoGEF2 and/or RhoGAP71E. In sum, these results provide a starting point for the revelation of the regulatory networks that guide these intermediaries to differential developmental outcomes.

Furthermore, our data indicate that tuning of pulsing dynamics by Rho1 and its regulators is crucial for the cells to maintain their shape and position in the lattice and prevent catastrophic tissue ruptures during this period of eye development. However, it is interesting to note that with constitutively active MLCK, we continued to observe pulsing accumulation of MyoII, even though the tissue architecture was highly disrupted. This observation is consistent with the idea that a core of pulsing dynamics may arise from the intrinsic biophysical properties of contractile actomyosin networks, wherein as F-actin filaments are exposed to high tension, they spontaneously disassemble (Haviv et al., 2008; Munjal et al., 2015). However, our results would also support the idea that pulsing characteristics are very finely tuned to work in balance with other processes occurring in the epithelium to maintain tissue structure and generate the appropriate developmental pattern.

A salient feature of retinal development is the continual movement and shape changes of cells, even though it takes hours for persistent changes to unfold. Our results suggest that continuous cycling of the nucleotide state of the Rho1 GTPases drives Rho1-dependent regulation of the cytoskeleton that underlies components of these movements. Thus, these are active, energy-dependent processes that cells invest in, despite the apparent transience of shape changes seen over the short term. There are various explanations for why medioapical actomyosin pulsing exists in other systems, for example, to enable apical constriction by ratcheting or to utilize the relaxation phase for plasma membrane remodeling to remove membrane and junctional proteins (Jewett et al., 2017;

Miao et al., 2019). Here in the *Drosophila* retina, it appears medioapical actomyosin pulsing coordinates the mechanical behavior of neighboring cells and functions to maintain mechanical tissue integrity. Previously, we described oscillations of junctional networks of LC-LC contacts that occurred with a periodicity of about 15 minutes (Del Signore et al., 2018; Malin et al., 2022). Here, pulsing of medioapical actomyosin networks has a periodicity closer to 6 minutes. While we do not yet know how these processes interplay, it is intriguing to note the existence of multiple sinusoidal functions that could distribute mechanical forces and speculate on how their actions are eventually integrated to generate the precise patterning of the eye.

Concluding remarks

We identified a pulsatile medioapical actomyosin network in LCs that exerts tension on the apical cell surface in a pattern that predicts the final shape changes of the cells. This network assembles into nodes connected by F-actin filaments that exert tension on one another and the cell surface. The network assembly is controlled by cell-to-cell mechanical interactions and is modulated intracellularly by RhoGAP71E and RhoGEF2. These mechanical cell-to-cell interactions manifest in inversely synchronized cell-to-cell oscillations of actomyosin and the contraction of apical cell area (Fig. 7). Our research suggests that during epithelial remodeling, when the cells are dynamically in pursuit of stable forms and stable interaction with neighbors, finely tuned pulsing of medioapical actomyosin networks functions in balancing the forces between epithelial cells. Regulated by mechanical and biochemical signals, Rho1 plays a crucial role in this delicate rebalancing act.

ACKNOWLEDGEMENTS

We thank J. Treisman, U. Tepass, A. Martin and J. Zallen for generous gifts of flies, the Bloomington Stock Center, the Vienna Drosophila Research Center, the Kyoto Stock Center for flies, and the Developmental Studies Hybridoma Bank for antibodies. We thank K. G. Commons for her critical reading of the manuscript and Paul Hatini for writing the R-script to perform Pearson's time correlation analysis. This work was supported by grants from the National Institute of Health to V.H. (R01 GM129151).

METHODS

Fly strains

To examine the *RhoGEF2* loss-of-function phenotypes, we employed the *RhoGEF2* ^{e037754} alleles. To examine the *RhoGEF2* overexpression phenotypes, we expressed *UAS-RhoGEF2* protein with the N-terminal T7 tag. To determine if *RhoGAP71E* GAP activity affects epithelial remodeling, we constructed a WT UAS- *RhoGAP71E* and a UAS-*RhoGAP71E* (R77A), a point mutant that disrupts the GAP activity. We selected UAS-insertions with similar expression levels to determine if these variants can rescue the *RhoGAP71E* clonal phenotypes using the MARCM technique. We employed a *RhoGAP71E*::GFP driven by the ubiquitin promoter to examine *RhoGAP71E* protein distribution and dynamics, and *RhoGAP71E*^{j6B9} FRT80B to generate genetically marked mutant clones.

Fly lines from the Bloomington *Drosophila* Stock Center: (1) Rho1::GFP (2) Rho1.N17, (3) Rho1 (4) MLCK.Ct, (5) Dia.CA , (6) UAS-T7.RhoGEF2, (7) UAS-Lifeact::Ruby, (8) sqh-GFP::Rok, (9) GMR-GAL4, (10) *y w*; Actin>y+>GAL4, UAS-GFP, (11) *w;* Actin>CD2stop>GAL4, UAS-mRFP, (12) *y w*; α-Cat::GFP^{gfstf}, (13) *y w* hsFLP; UAS-GFP^{nls}, (14) *w;* tub-GAL4; FRT40A, tub-GAL80^{ts}, (15) *w Ey*Flp; FRT42D, GMR-myr::mRFP, (16) *w;* FRT80B, Ubi-GFP, (17) RhoGEF2-RNAi and (18) RhoGAP71E-RNAi. α-Cat::Venus^{CPTI002596} and *RhoGAP71E* ^{j6B9} 80B were obtained from the Kyoto stock center. Fly lines previously described by Del Signore et. al. (2018) and Malin et al. (2022): (1) GMR-GAL4, α-Cat::Venus,

(2) UAS-Lifeact::Ruby; GMR-GAL4, (3) UAS-Lifeact::GFP; sqh-Sqh::mCherry, GMR-GAL4, (4) UAS-Lifeact::Ruby; sqh-Rok::GFP, GMR-GAL4, Additional stocks used: (1) sqh-Sqh::mCherry and (2) sqh-UtrABD::GFP, sqh-Sqh::mCherry (gift of A. Martin), (3) GMR-GAL4, UAS–α-Cat::GFP (gift of R. Cagan). RhoGAP71E::GFP and RhoGEF2::GFP (A. Martin).

Molecular biology and construction of genetically encoded reporters – We generated several new reporters driven by the UAS and the ubiquitin promoter including Ubi-RhoGAP71E::GFP, UAS-RhoGAP71E::GFP. The *RhoGAP71E* open reading frame (ORF) was amplified from cDNA clone LD04071. The PCR products were inserted into the pENTR plasmid by Topo cloning. All expression clones were generated by the Gateway technology (Walhout et al. 2000) using the *Drosophila* Gateway Vector Collections (gift of T. Murphy and C.-Y. Pay) using the Clonase II reaction to fuse the ORFs in frame with a desired fluorescent protein. Site-directed mutagenesis using QuickChange II site-directed mutagenesis was performed to inactivate GAP activity of RhoGAP71E by substituting an arginine as position 77 to alanine to generate UAS-RhoGAP71E::GFP (R77A). Transgenic flies carrying these transgenes were established by standard methods by BestGene Inc.

Genetic analysis

GMR-GAL4 was used to broadly express UAS-transgenes in the eye (Wernet et al., 2003). The FLP/FRT (Xu & Rubin, 1995), and MARCM techniques (Lee and Luo, 2001) were used to generate genetically marked clones by FLP-mediated mitotic recombination and the FLP-Out/GAL4 technique to expressed desired transgene in genetically marked clones. y w hsFLP; Ubi-mRFP, FRT42D and y w hsFLP; Ubi-GFP, FRT80B were used to generate *RhoGE2* and *RhoGAP71E* mutant FLP/FRT clones, and eyFLP, tub-GAL80 UAS-GFP; tub-GAL4 FRT40A to generate MARCM clones. Mitotic clones were induced by a heat shock for 30 minutes at 34°C.

METHOD DETAILS

Immunofluorescence

White prepupae (0h APF) were selected and aged on glass slides in a humidifying chamber at 25°C. Pupal eyes were dissected in phosphate buffered saline, fixed for 35 minutes in 4% paraformaldehyde in PBS and stained with antibodies in PBS with 3% BSA, 0.3% Triton X-100 and 0.01% Sodium Azide. Primary antibodies used were rat anti-E-cad (DSHB #DCAD2, 1:100), mouse anti-Dlg (DSHB #4F3, 1:500) and guinea pig anti-Sqh1P (gift from R. Ward). Alexa 405 (Calbiochem), Alexa488, Alexa647 (Molecular Probes), and Cy3 and Cy5 (Jackson ImmunoResearch) conjugated secondary antibodies were used at 1:150.

Confocal time-lapse imaging

Flies were selected for imaging at 28h APF at 25c unless described otherwise. Pupae were mounted in a slit created in an agarose block with eyes facing the coverslip after the operculum for each pupa was removed. The agarose block was surrounded by a rubber gasket prepared in the lab and capped with a custom-built humidified chamber. Time-lapse imaging was performed on a Zeiss LSM800 inverted laser scanning confocal microscope. Images were taken every 5, 30, and 60 sec as noted with an optimal pinhole (1 AU) using a 63x, 1.4-NA, plan Apochromat immersion objective, 0.7 µm per optical section with a 10–50% overlap between sections, at a scan speed of 6-7.

Laser ablation

Laser nano-ablations to probe tissue mechanics were performed using a Zeiss LSM880 NLO with a near-infrared InSight X3 two-photon tunable laser (680-1300nm) using a 740nm multiphoton excitation. Samples were imaged with Utr::GFP and Sqh::mCh to identify the medioapical actomyosin network for ablation using a 63X oil immersion objective (N.A 1.4). A small field size, of 4X4 pixels, was ablated in the center of either a 2° or a 3° LCs using a 30-40% laser output, at a scan of one, with one

iteration. Images were collected every second for 200 sec in a frame of 1584x1584 pixels to aid with the scan speed. Ablations were performed 6 seconds after the beginning of each experiment.

Quantification and Statistical Analysis

Cell expansion analysis

The areas of the 2° and 3° LCs were measured before and 180 seconds after ablation to calculate the fold expansion of the apical cell area in Fiji. Ratios were calculated in Microsoft Excel by dividing the total area after ablation over the area pre-ablation. Data were plotted in GraphPad Prism 9. 2°-3°, 2°-1°, and 3°-1 contacts lengths for both 2° and 3° LCs were also measured before ablation and 180 seconds after ablation. Ratios were also calculated in Microsoft excel by dividing the total contact lengths after ablation over the length pre-ablation. Ratios were plotted in GraphPad Prism 9 and compared to normalized contact fold change close to 1 before ablation.

Correlation analysis of apical cell area vs. signal intensity of fluorescent proteins

We analyzed the changes in F-actin (using Utr::GFP), MyoII using MyoII::mCh, RhoGEF2::GFP and RhoGAP71E::GFP intensity at around 28h APF, during the remodeling process of the 2° LCs in time-lapse movies with a time resolution of 5 seconds. Using the Fiji polygon selection tool, we traced manually individual apical perimeters of 2° LCs. ROIs were generated, and minimum, maximum, and mean average intensity were obtained for each cell and normalized against the background. Using a custom R-script we measured the time-resolved Pearson's cross-correlations (time windows from ±8 min) between the mean signal intensities of the fluorescent reporter and cell area using 20–30-min-long movies. The data were smoothed using an "R" kernel regression smoother and presented as the average Pearson's correlation of individual cells and standard error of the mean. Statistics were performed on the average R-value changes for apical cell area vs. RhoGEF2::GFP, apical cell area vs. RhoGAP71E::GFP, apical cell area vs. Utr::GFP, Utr::GFP and Sqh::mCh, apical cell area vs. MyoII in Act>RhoGAP71E RNAi and RhoGEF2 RNAi expressing cells using the one-sample t-Test with a

theoretical mean of 0. Pulse duration was obtained after plotting the apical cell area against time. Distances between the maxima were obtained and averaged. Amplitudes were obtained by calculating the distance between the maxima and minima to obtain an average amplitude or fold-change of signal intensity. For the cell-to-cell comparisons, R-values were generated for the correlation between areas of adjacent 2° LCs and between cell area of one cell and actin intensity in the neighboring cells. R-values were averaged, and a one-sample-t-Test was performed against a theoretical mean of 0.

Comparing signal intensities between WT and RhoGAP71E RNAi expressing cell clones

LCs were selected for analysis if all adjacent cells were mutant, or, for the control group, if all adjacent cells were WT. For each 2° LCs, circular ROIs were used to measure the signal intensity at the medioapical region from which the background was subtracted to calculate the average signal intensity in RhoGAP71E RNAi and WT LCs. A t-test for normally distributed data and a Mann-Whitney test for non-normally distributed data was used to compare the groups.

REFERENCES

Azevedo, D., M. Antunes, S. Prag, X. Ma, U. Hacker, G.W. Brodland, M.S. Hutson, J. Solon, and A. Jacinto. 2011. DRhoGEF2 regulates cellular tension and cell pulsations in the Amnioserosa during *Drosophila* dorsal closure. *PLoS One*. 6:e23964.

Bao, S., and R. Cagan. 2005. Preferential adhesion mediated by Hibris and Roughest regulates morphogenesis and patterning in the *Drosophila* eye. *Dev Cell*. 8:925-935.

Bao, S., K.F. Fischbach, V. Corbin, and R.L. Cagan. 2010. Preferential adhesion maintains separation of ommatidia in the *Drosophila* eye. *Dev Biol*. 344:948-956.

Blackie, L., M. Tozluoglu, M. Trylinski, R.F. Walther, F. Schweisguth, Y. Mao, and F. Pichaud. 2021. A combination of Notch signaling, preferential adhesion and endocytosis induces a slow mode of cell intercalation in the *Drosophila* retina. *Development*. 148.

Blackie, L., R.F. Walther, M.F. Staddon, S. Banerjee, and F. Pichaud. 2020. Cell-type-specific mechanical response and myosin dynamics during retinal lens development in *Drosophila*. *Mol Biol Cell*. 31:1355-1369.

Blanchard, G.B., S. Murugesu, R.J. Adams, A. Martinez-Arias, and N. Gorfinkiel. 2010. Cytoskeletal dynamics and supracellular organisation of cell shape fluctuations during dorsal closure. *Development*. 137:2743-2752.

Cagan, R. 2009. Principles of *Drosophila* eye differentiation. *Curr Top Dev Biol*. 89:115-135.

Cagan, R.L., and D.F. Ready. 1989. The emergence of order in the *Drosophila* pupal retina. *Dev Biol*. 136:346-362.

Carthew, R.W. 2007. Pattern formation in the *Drosophila* eye. *Curr Opin Genet Dev*. 17:309-313.

Chanet, S., C.J. Miller, E.D. Vaishnav, B. Ermentrout, L.A. Davidson, and A.C. Martin. 2017. Actomyosin meshwork mechanosensing enables tissue shape to orient cell force. *Nat Commun*. 8:15014.

Christodoulou, N., and P.A. Skourides. 2015. Cell-Autonomous Ca(2+) Flashes Elicit Pulsed Contractions of an Apical Actin Network to Drive Apical Constriction during Neural Tube Closure. *Cell Rep*. 13:2189-2202.

Collinet, C., M. Rauzi, P.F. Lenne, and T. Lecuit. 2015. Local and tissue-scale forces drive oriented junction growth during tissue extension. *Nat Cell Biol*. 17:1247-1258.

del Rio, A., R. Perez-Jimenez, R. Liu, P. Roca-Cusachs, J.M. Fernandez, and M.P. Sheetz. 2009. Stretching single talin rod molecules activates vinculin binding. *Science*. 323:638-641.

Del Signore, S.J., R. Cilla, and V. Hatini. 2018. The WAVE Regulatory Complex and Branched F-Actin Counterbalance Contractile Force to Control Cell Shape and Packing in the *Drosophila* Eye. *Dev Cell*. 44:471-483 e474.

Denk-Lobnig, M., J.F. Totz, N.C. Heer, J. Dunkel, and A.C. Martin. 2021. Combinatorial patterns of graded RhoA activation and uniform F-actin depletion promote tissue curvature. *Development*. 148 (11):dev199232.

Etienne-Manneville, S., and A. Hall. 2002. Rho GTPases in cell biology. *Nature*. 420:629-635.

Fernandez-Gonzalez, R., and J.A. Zallen. 2011. Oscillatory behaviors and hierarchical assembly of contractile structures in intercalating cells. *Phys Biol*. 8:045005.

Fox, D.T., and M. Peifer. 2007. Abelson kinase (Abl) and RhoGEF2 regulate actin organization during cell constriction in *Drosophila*. *Development*. 134:567-578.

Gaertner, F., P. Reis-Rodrigues, I. de Vries, M. Hons, J. Aguilera, M. Riedl, A. Leithner, S. Tasciyan, A. Kopf, J. Merrin, V. Zheden, W.A. Kaufmann, R. Hauschild, and M. Sixt. 2022. WASp triggers mechanosensitive actin patches to facilitate immune cell migration in dense tissues. *Dev Cell*. 57:47-62 e49.

Greenberg, L., and V. Hatini. 2011. Systematic expression and loss-of-function analysis defines spatially restricted requirements for *Drosophila* RhoGEFs and RhoGAPs in leg morphogenesis. *Mech Dev*. 128:5-17.

Hacker, U., and N. Perrimon. 1998. DRhoGEF2 encodes a member of the Dbl family of oncogenes and controls cell shape changes during gastrulation in *Drosophila*. *Genes Dev*. 12:274-284.

Haviv, L., D. Gillo, F. Backouche, and A. Bernheim-Groswasser. 2008. A cytoskeletal demolition worker: myosin II acts as an actin depolymerization agent. *J Mol Biol*. 375:325-330.

Hayashi, T., and R.W. Carthew. 2004. Surface mechanics mediate pattern formation in the developing retina. *Nature*. 431:647-652.

He, L., X. Wang, H.L. Tang, and D.J. Montell. 2010. Tissue elongation requires oscillating contractions of a basal actomyosin network. *Nat Cell Biol*. 12:1133-1142.

Homem, C.C., and M. Peifer. 2008. Diaphanous regulates myosin and adherens junctions to control cell contractility and protrusive behavior during morphogenesis. *Development*. 135:1005-1018.

Jaffe, A.B., and A. Hall. 2005. Rho GTPases: biochemistry and biology. *Annu Rev Cell Dev Biol*. 21:247-269.

Jewett, C.E., T.E. Vanderleest, H. Miao, Y. Xie, R. Madhu, D. Loerke, and J.T. Blankenship. 2017. Planar polarized Rab35 functions as an oscillatory ratchet during cell intercalation in the *Drosophila* epithelium. *Nat Commun*. 8:476.

Johnson, R.I. 2021. Hexagonal patterning of the *Drosophila* eye. *Dev Biol*. 478:173-182.

Johnson, R.I., M.J. Seppa, and R.L. Cagan. 2008. The *Drosophila* CD2AP/CIN85 orthologue Cindr regulates junctions and cytoskeleton dynamics during tissue patterning. *J Cell Biol*. 180:1191-1204.

Jordan, P., and R. Karess. 1997. Myosin light chain-activating phosphorylation sites are required for oogenesis in *Drosophila*. *J Cell Biol*. 139:1805-1819.

Kasza, K.E., D.L. Farrell, and J.A. Zallen. 2014. Spatiotemporal control of epithelial remodeling by regulated myosin phosphorylation. *Proc Natl Acad Sci U S A*. 111:11732-11737.

Larson, D.E., Z. Liberman, and R.L. Cagan. 2008. Cellular behavior in the developing *Drosophila* pupal retina. *Mech Dev*. 125:223-232.

Lee, T., and L. Luo. 2001. Mosaic analysis with a repressible cell marker (MARCM) for *Drosophila* neural development. *Trends Neurosci*. 24:251-254.

Letizia, A., D. He, S. Astigarraga, J. Colombelli, V. Hatini, M. Llimargas, and J.E. Treisman. 2019. Sidekick Is a Key Component of Tricellular Adherens Junctions that Acts to Resolve Cell Rearrangements. *Dev Cell*. 50:313-326 e315.

Magie, C.R., M.R. Meyer, M.S. Gorsuch, and S.M. Parkhurst. 1999. Mutations in the Rho1 small GTPase disrupt morphogenesis and segmentation during early *Drosophila* development. *Development*. 126:5353-5364.

Maitre, J.L., R. Niwayama, H. Turlier, F. Nedelec, and T. Hiiragi. 2015. Pulsatile cell-autonomous contractility drives compaction in the mouse embryo. *Nat Cell Biol*. 17:849-855.

Malin, J., C. Rosa Birriel, S. Astigarraga, J.E. Treisman, and V. Hatini. 2022. Sidekick dynamically rebalances contractile and protrusive forces to control tissue morphogenesis. *J Cell Biol*. 221 (5):e202107035.

Martin, A.C., M. Gelbart, R. Fernandez-Gonzalez, M. Kaschube, and E.F. Wieschaus. 2010. Integration of contractile forces during tissue invagination. *J Cell Biol*. 188:735-749.

Martin, A.C., M. Kaschube, and E.F. Wieschaus. 2009. Pulsed contractions of an actin-myosin network drive apical constriction. *Nature*. 457:495-499.

Mason, F.M., S. Xie, C.G. Vasquez, M. Tworoger, and A.C. Martin. 2016. RhoA GTPase inhibition organizes contraction during epithelial morphogenesis. *J Cell Biol*. 214:603-617.

Miao, H., T.E. Vanderleest, C.E. Jewett, D. Loerke, and J.T. Blankenship. 2019. Cell ratcheting through the Sbf RabGEF directs force balancing and stepped apical constriction. *J Cell Biol*. 218:3845-3860.

Mizuno, T., M. Amano, K. Kaibuchi, and Y. Nishida. 1999. Identification and characterization of *Drosophila* homolog of Rho-kinase. *Gene*. 238:437-444.

Mueller, J., G. Szep, M. Nemethova, I. de Vries, A.D. Lieber, C. Winkler, K. Kruse, J.V. Small, C. Schmeiser, K. Keren, R. Hauschild, and M. Sixt. 2017. Load Adaptation of Lamellipodial Actin Networks. *Cell*. 171:188-200 e116.

Mulinari, S., M.P. Barmchi, and U. Hacker. 2008. DRhoGEF2 and diaphanous regulate contractile force during segmental groove morphogenesis in the *Drosophila* embryo. *Mol Biol Cell*. 19:1883-1892.

Munjal, A., J.M. Philippe, E. Munro, and T. Lecuit. 2015. A self-organized biomechanical network drives shape changes during tissue morphogenesis. *Nature*. 524:351-355.

Rauzi, M., P.F. Lenne, and T. Lecuit. 2010. Planar polarized actomyosin contractile flows control epithelial junction remodelling. *Nature*. 468:1110-1114.

Ridley, A.J., and A. Hall. 1992. The small GTP-binding protein rho regulates the assembly of focal adhesions and actin stress fibers in response to growth factors. *Cell*. 70:389-399.

Sawyer, J.K., W. Choi, K.C. Jung, L. He, N.J. Harris, and M. Peifer. 2011. A contractile actomyosin network linked to adherens junctions by Canoe/afadin helps drive convergent extension. *Mol Biol Cell*. 22:2491-2508.

Seppa, M.J., R.I. Johnson, S. Bao, and R.L. Cagan. 2008. Polychaetoid controls patterning by modulating adhesion in the *Drosophila* pupal retina. *Dev Biol*. 318:1-16.

Solon, J., A. Kaya-Copur, J. Colombelli, and D. Brunner. 2009. Pulsed forces timed by a ratchet-like mechanism drive directed tissue movement during dorsal closure. *Cell*. 137:1331-1342.

Spadaro, D., S. Le, T. Laroche, I. Mean, L. Jond, J. Yan, and S. Citi. 2017. Tension-Dependent Stretching Activates ZO-1 to Control the Junctional Localization of Its Interactors. *Curr Biol*. 27:3783-3795 e3788.

Stowers, R.S., and T.L. Schwarz. 1999. A genetic method for generating *Drosophila* eyes composed exclusively of mitotic clones of a single genotype. *Genetics*. 152:1631-1639.

Vanderleest, T.E., C.M. Smits, Y. Xie, C.E. Jewett, J.T. Blankenship, and D. Loerke. 2018. Vertex sliding drives intercalation by radial coupling of adhesion and actomyosin networks during *Drosophila* germband extension. *Elife*. 7:e34586.

Vasquez, C.G., M. Tworoger, and A.C. Martin. 2014. Dynamic myosin phosphorylation regulates contractile pulses and tissue integrity during epithelial morphogenesis. *J Cell Biol*. 206:435-450.

Warner, S.J., and G.D. Longmore. 2009a. Cdc42 antagonizes Rho1 activity at adherens junctions to limit epithelial cell apical tension. *J Cell Biol*. 187:119-133.

Warner, S.J., and G.D. Longmore. 2009b. Distinct functions for Rho1 in maintaining adherens junctions and apical tension in remodeling epithelia. *J Cell Biol*. 185:1111-1125.

Wernet, M.F., T. Labhart, F. Baumann, E.O. Mazzoni, F. Pichaud, and C. Desplan. 2003. Homothorax switches function of *Drosophila* photoreceptors from color to polarized light sensors. *Cell*. 115:267-279.

Xie, S., and A.C. Martin. 2015. Intracellular signalling and intercellular coupling coordinate heterogeneous contractile events to facilitate tissue folding. *Nat Commun*. 6:7161.

Yonemura, S., Y. Wada, T. Watanabe, A. Nagafuchi, and M. Shibata. 2010. alpha-Catenin as a tension transducer that induces adherens junction development. *Nat Cell Biol*. 12:533-542.

Yu, J.C., and R. Fernandez-Gonzalez. 2016. Local mechanical forces promote polarized junctional assembly and axis elongation in *Drosophila*. *Elife*. 5:e10757.

FIGURE LEGENDS

Figure 1: A dynamic medioapical actomyosin network correlates with cell area fluctuations during epithelial remodeling. (A) Left: Cartoon of *Drosophila* ommatidium during pruning and shape changes; Right: A key for the cell types and dynamics in this and subsequent images. (B) Medioapical actomyosin dynamics in LCs during cell shape changes. Top: Snapshots of a lattice edge highlight the assembly (red arrow) and disassembly (green arrow) of a medioapical actomyosin ring. Bottom: Zoomed-in images of F-actin and MyoII dynamics. Red bars: Assembly of a medioapical ring; Green bar: Ring disassembly. (B') Medioapical F-actin and MyoII accumulation are positively correlated (B") F-actin and cell area negatively correlate at a peak of -15 sec. The black line represents the mean R-value at each time shift, and the green overlay shows the SE of the mean. (C) F-actin (Lifeact::Ruby) and Rok::GFP dynamics in LCs. Top: Snapshots from a time-lapse movie. Bottom: A kymograph of medioapical F-actin and Rok::GFP dynamics in LCs. Yellow arrows: Medioapical Rok::GFP accumulation. (D) Dynamic medioapical Rho1::GFP accumulation. Top: Snapshots from time-lapse movies. Bottom: Kymographs of medioapical F-actin and Rho1::GFP in a LC. Yellow arrows: medioapical Rho1::GFP accumulation. (E-E'') Kymographs show three distinct behaviors of the medioapical actomyosin network: (E) Assembly of a medioapical ring (red arrow) during contraction of a LC. (E') Movement and fusion of F-actin nodes marked with arrows. (E") Movement of nodes and fusion with the junctional actomyosin network. A subset of F-actin nodes (marked by the yellow ellipse) flow toward the LC-LC contact, marked by white arrows. (F) Medioapical F-actin pulse frequency in WT 2° LCs (peak to peak) is approximately 6 minutes (349 +/- 96 sec, N=11). (G) The peak levels of medioapical F-actin are, on average 1.4-fold higher than the trough levels.

Figure 2: The medioapical actomyosin network holds tension and mechanically links the lattice cells. (A-B) High-resolution Airyscan images of F-actin (Lifeact::GFP) and MyoII (MyoII::mCh) from a time-lapse movie. Medioapical actomyosin nodes connect to cell contacts through filamentous structures (yellow arrowheads). (B-E) Targeted ablations (marked with a yellow star) of the medioapical

actomyosin in LCs induced a rapid apical cell area relaxation. (B) Medioapical actomyosin ablation in 2° LCs induced preferential expansion of the 2°-3° contact and flow of the actomyosin network toward the LC-LC contacts, concomitant with apical area relaxation, and increased actomyosin levels at LC-LC contacts. Top: Snapshots from a time-lapse movie of a lattice edge; Bottom: Zoom-in views of F-actin and MyoII in the boxed area. Note a flow of F-actin (marked by the ellipse) towards the LC-LC contacts (marked by the white arrow). (C) Partial medioapical actomyosin ablation resulted in a weaker apical area relaxation and recoil of actomyosin to LC-LC contacts (white arrow). (D) Ablation of the medioapical actomyosin in 3° LCs induces a strong relaxation of the apical cell area and a preferential expansion of 3°-1° contacts compared to 3°-2° contacts. Vertices of the ablated 3° LC are marked with yellow arrowheads. (E) Top panel: Fold change of the 2° LC area and cell-cell contacts after ablation. Two-way ANOVA was performed with Two-way ANOVA was performed with Sídák's multi-comparison to compare each data set before to after ablation. 2° LCs' area after ablation vs. before ablation, $p<0.0001$, N=10. 2°-3° contact length after ablation vs. before ablation, $p<0.0001$, N=10. 2°-1° contact length after ablation vs. before ablation, $p=0.1569$, N=10. Bottom Panel: Fold change of the 3° cell area and cell-cell contact before and after ablation. Two-way ANOVA was performed to compare each data set before to after ablation. 3° LCs' area after ablation vs. before ablation, $p<0.0001$, N=8. 3°-2° contact length after ablation vs. before ablation, $p=0.0015$, N=8. 3°-1° contact length after ablation vs. before ablation, $p<0.0001$, N=8. (F) A cartoon depicting the forces that regulate cell shape inferred from the pattern of recoil of 2° and 3° LCs after laser ablation. Red arrows depict contractile forces, and their thickness represents their magnitude. Green arrows depict the passive stretching of the 2°-1° cell contacts in response to the contraction of the 3° LCs. (G) After ablation of a 2° LC (marked with a star), the apical area of the adjacent 3° expands. This is followed by an increase in medioapical actomyosin and cell area contraction (red arrow). Top: Snapshots from a time-lapse movie of a lattice edge before and after 2° LC ablation. Bottom: Zoom-in view of F-actin and MyoII.

Figure 3: Rho1 regulates medioapical actomyosin dynamics and cell area fluctuations. (A) F-actin organization and dynamics in Rho1^{DN} expressing eyes. Top: Snapshots of a lattice edge. The continuity of the junctional actomyosin network is interrupted (white arrow). Bottom: Zoomed-in images of the 2° LCs (boxed area) show dynamic assembly and disassembly of the medioapical F-actin network correlating with cell area contraction (red arrows) and expansion (green arrows), respectively. Yellow arrowheads demarcate LC-LC contacts. (B-C) Conditional Rho1 overexpression promotes medioapical F-actin dynamics and cell area fluctuations. (B) Kymograph shows F-actin node fusion (tracked by the yellow arrows) promoting medioapical F-actin ring formation (red arrow). (C) A kymograph showing changes in medioapical F-actin in a cell that overexpresses Rho1. Green arrows, low F-actin intensity and cell area relaxation; red arrows, high F-actin intensity and cell area contraction. (C') Medioapical F-actin pulse frequency, from peak to peak, in the 2° LCs is approximately 2 minutes (245 +/- 50 sec, N=16). (C") Medioapical F-actin increases on average 4.5-fold (N=14) from trough to peak in the 2° LCs. (C''') Time correlation shows that medioapical F-actin levels negatively correlate with the apical cell area of 2° LCs. (D) The peak correlation between F-actin and cell area in Rho1 expressing eyes is significantly higher than in WT (R= -0.6508 at peak correlation of -15sec, N=15, t-Test p= 0.0002). (E) Contractile medioapical actomyosin dynamics and cell area fluctuations inversely coordinate between adjacent 2° cells prior to cell pruning. (E') Cell area of adjacent 2° LCs is negatively correlated (R=-0.2020 at a peak correlation of +15 sec, N=7 (14 pairs), one-sample t-Test; p= 0.0318). (F) A model describing the cell-to-cell force rebalancing observed in LCs. Retinas were imaged every minute in panel A and every 5 seconds in panels B-D.

Figure 4: MyoII and F-actin turnover affect medioapical contractile dynamics. (A) A diagram of the Rho1 GTPase pathway in the regulation of actomyosin contractility. Epithelial organization labeled with α-cat::GFP in (B) WT, and (C) MLCK^{CA} and (D) Dia^{CA} expressing eyes. (C) MLCK^{CA} expression disrupted cell intercalation resulting in clustering of 2° LCs around mechanosensory bristles (yellow arrow). The AJs appeared fragmented, holes formed in the tissue (marked with yellow dotted lines)

and cone cells cavitated (white arrow). (D) Dia^{CA} expression also led to a partial fragmentation of the AJs and cavitation of the cone cells. (E) MLCK^{CA} expression significantly decreased the apical cell area of 2° LCs (t-test, p <0.0001, N=15), while Dia^{CA} expression increased apical cell area compared with WT (t-test, p<0.0001, N=15). (F) MLCK^{CA} expression increased medioapical MyoII dynamics. Top: Snapshots of a lattice edge from a time-lapse movie where the cells express MyoII::mCh; Bottom: Zoom-in views of MyoII alone in the boxed area every minute. Note the pulsatile assembly and disassembly of a MyoII ring. (F') The frequency of medioapical MyoII pulsing is, on average, 10 minutes +/- 2.5min (N=10, 30 pulses). (F") Medioapical MyoII levels and the apical area of 2° LCs negatively correlate (R= -0.2126, One-sample t-Test, p=0.0044, N=15) (G) Dia^{CA} expression remodels F-actin to a thick band at the cell periphery and leads to the loss of medioapical actomyosin assembly. Top: Snapshots of a lattice edge expressing Utr::GFP from a time-lapse movie. Bottom: Zoomed-in views of F-actin in the boxed area.

Figure 5: RhoGEF2 promotes medioapical actomyosin network turnover. (A) RhoGEF2::GFP and F-actin labeled with Lifeact::Ruby. Snapshots from a time-lapse movie of a lattice edge (top) and magnified views of a 2° LC demarcated with a box. RhoGEF2::GFP (yellow arrow) accumulates medioapically in pulses. (A') RhoGEF2::GFP accumulation correlates negatively with cell area at a peak of + 15 sec (R= -0.1361, N=12, one-sample t-Test p=0.0250). (B-C) *RhoGEF2* loss affects tissue integrity and medioapical MyoII dynamics. (B) Left: Merge image of patches of negatively marked *RhoGEF2* mutant cells expressing MyoII::GFP. Middle: The dotted lines demarcate patches of positively marked *RhoGEF2* mutant clone cells. Note the patterning defect in the mutant cells (inside the yellow dotted region) compared with WT cells (RFP^{+}). (C) Sparse actomyosin assembly in *RhoGEF2* mutant cells (white arrow) compared with the adjacent WT cell (yellow arrow). (C') Left: Time correlation plot between medioapical MyoII levels and apical area in *RhoGEF2* mutant LCs. Right: Correlation is lost in the *RhoGEF2* mutant cells (one-sample t-Test, R= -0.01945, N=14 p=0.5673). (D) Depletion of *RhoGEF2* by RNAi reduces medioapical MyoII assembly compared with the WT counterpart. (D'-D") Kymograph

shows a reduction in MyoII levels in the RhoGEF2RNAi expressing cells compared with WT (D’’’) Left: Time correlation plots between medioapical MyoII levels and LCs area in WT (green) and RhoGEF2RNAi expressing cells (pink). Right: Correlation is weaker in RhoGEF2 RNAi expressing 2° LCs compared with the WT counterparts (paired t-test, p=0.0281, N=8 pairs). (E) RhoGEF2 expression enhanced medioapical actomyosin network assembly and apical cell area fluctuations. Top: Snapshots of a lattice edge. Bottom: Magnified views of the 2° LC (white box) show the assembly (red arrow) and disassembly (green arrow) of the medioapical actomyosin network that correlates with cell area contraction and expansion, respectively. (E’) Medioapical F-actin levels correlate with apical area contraction 2° LCs. (E") Medioapical F-actin pulse duration is approximately 2 minutes (215+/- 56 sec (N=12). (F) RhoGEF2 expression increases the peak correlation between F-actin and cell area (peak correlation of -15 sec, N=11, t-Test p= 0.0337). (G) Rho1 and RhoGEF2 expression increase the (G) pulse frequency and (H) pulse amplitude of F-actin accumulation compared with WT. (G) One-way ANOVA with Tukey’s multiple comparisons was performed. WT vs. GMR>Rho1, mean difference of 104 sec, p=0.0010. WT vs. GMR>RhoGEF2, mean difference 133 sec, p=0.0001. GMR>Rho1 vs. GMR>RhoGEF2, mean difference 29 sec, p=0.5084, N=11-16. (H) Welch One-way ANOVA with Dunnett’s comparison between WT and GMR>Rho1, mean difference of R= -0.3139, p<0.0001. WT vs. GMR>RhoGEF2, mean difference of R= -0.6155, p= 0.0218. GMR>Rho1 vs. GMR>RhoGEF2, mean difference of R= 2.523, p= 0.0011, N=14.

Figure 6: RhoGAP71E promotes the disassembly of the medioapical actomyosin network. (A) RhoGAP71E::GFP accumulated medioapically in pulses (yellow arrow). Snapshots from a time-lapse movie of an ommatidium (Left), lattice edge (top), and magnified views of a 2° LC demarcated with a box. (A’) Medioapical RhoGAP71E::GFP levels negatively correlate with apical cell area of 2° LCs. Left: Peak correlation occurs at a time shift of + 10 sec (R= -0.1399, N=11, one-sample t-Test p=0.0328). (B-D) RhoGAP71E promotes apical cell area expansion. (B) *RhoGAP71E* mutant cells marked by GFP in fixed tissue stained for E-cadherin. White arrows mark WT LCs; yellow arrows and arrowheads mark

mutant LCs. 1° LCs are marked by arrowheads and 2° LCs by arrows. (B') The Apical area of the *RhoGAP71E* mutant cells is significantly smaller than the area of WT counterparts (Paired t-Test, p= 0.0007, N=10 pairs) (C) *RhoGAP71E* inhibits MyoII phosphorylation and activation. RhoGAP71E RNAi expressing clones in fixed tissue stained for phosphorylated MyoII (p-MyoII). (C') p-MyoII levels are higher in the clones (C") compared with the WT regions. (C'") T-test, p<0.0001, N=6. (D) RhoGAP71E RNAi expression decreases apical cell area. Left: Merge snapshot from a time-lapse movie of RhoGAP71E RNAi clones (RFP^+) expressing MyoII (Sqh::GFP). (D') Zoom-in view of a RhoGAP71E RNAi expressing 2° LC with reduced cell area compared with (D") a WT counterpart. (D''') Left: The peak negative correlation (at -15 sec) between MyoII accumulation and apical area is higher in RhoGAP71E RNAi expressing cells (light brown) compared with WT (green). Paired t-test, p=0.0127, N=10 pairs. Right: RhoGAP71E RNAi expression increased medioapical MyoII pulse frequency in the 2° LC to approximately 3 minutes (212 +/- 69sec,) compared with approximately 6.5 minutes in WT (387 +/- 177 sec, t-test, p= 0.0109, N=7). (E-F) Epithelial cell outlines labeled with α-Cat::GFP. (E) WT. (F) RhoGAP71E overexpression disrupted epithelial organization (yellow star) and caused expansion of the cells' apical area (yellow arrow) and gaps in the continuity of the AJs (yellow arrowhead). (F') RhoGAP71E expression significantly increased the apical cell area of 2° LC compared with WT (N=14, t-Test, p <0.0001). (G) RhoGAP71E expression reduced medioapical F-actin levels. Top: Snapshots of a lattice edge. Bottom: A magnified view of the 2° LC (white box). (G') Left: RhoGAP71E expression decreased medioapical F-actin assembly and actomyosin ring formation and abolished the correlation between actomyosin accumulation and cell area contraction. Right: Paired t-test at a time shift of -15 sec (p=0.0060, N=12 pairs). Yellow arrow, a faint actomyosin ring can be detected in LCs that failed to contract their apical cell area. White arrow, network disassembly did not lead to cell area expansion.

Figure 7: Regulated cell-to-cell coordination of mechanical behavior. A summary diagram of the results reported in this study. LCs are mechanically coupled, and their mechanical behavior is coordinated. The contraction of a LCs stretches the adjacent LC and promotes the disassembly of its

contractile medioapical actomyosin network. This is sensed by the stretched cell and leads to the assembly of a contractile network that contracts its apical area. Cell area contraction stretches the neighboring cells' apical area, promoting the disassembly of its medioapical actomyosin network, followed by reassembly to repeat the cycle. This cell-to-cell coordination of cytoskeletal and mechanical behavior is controlled by is dependent on dynamic Rho1 function and downstream effectors Dia and MyoII. Rho1 must be both activated by RhoGEF2 and inhibited by RhoGAP71E for these dynamics to occur.

SUPPLEMENTAL FIGURES

Figure S1: The assembly of a dynamic medioapical MyoII network correlates with cell area fluctuations during epithelial remodeling. (A) High-resolution Airyscan images of F-actin (Lifeact::GFP) and MyoII (MyoII::mCh) from a time-lapse movie. Note MyoII localization with F-actin filaments (yellow arrows). (B) An example of dynamic changes in MyoII and F-actin accumulation during LC remodeling. (B') Medioapical F-actin and MyoII positively correlate at 0 sec time-shift (R=0.4400, N=15 cells, one-sample t-Test: p <0.0001). (B'') Medioapical F-actin and apical cell area negatively correlate at a peak time shift of -15 sec (R= -0.2706, N=15 cells, one-sample t-Test: p= 0.0014). (C) Example of MyoII intensity correlation with cell area of a single LC. (C') One sample t-Test shows a significant negative correlation between medioapical MyoII levels and cell area (R= -0.2190, N= 11, p= 0.0482).

Figure S2: 1° and cone cells are mechanically coupled. (A-D) Rho1 expression promotes medioapical F-actin dynamics and cell area fluctuations that are inversely coordinated between adjacent cells. kymographs showing changes in medioapical F-actin in WT cone cells (A) and cone cells that express Rho1 (B). Green arrows, low F-actin intensity and cell area relaxation. Red arrows, high F-actin intensity and cell area contraction. (B') Fluctuations in F-actin levels are negatively correlated between anterior and posterior cone cells that express Rho1 (R= -0.4496, N= 16 cells, one-sample t-Test:

p=0.0086). (C) Kymographs of medioapical F-actin dynamics in the WT 1° LCs. (D) Fluctuations in F-actin also appear to be negatively correlated between adjacent 1° LCs that express Rho1.

Figure S3: RhoGEF2 rescues cellular defect caused by RhoGAP71E expression.

Epithelial organization in (A) In GMR>RhoGEF2 eyes epithelial cells maintain normal shape and rearrangements. (B) GMR>RhoGAP71E induces intercalation defects and expansion of the apical cell area. (C) Expressing RhoGEF2 with RhoGAP71E partially rescued the GMR>RhoGAP71E phenotypes. (D) Quantification of lattice defects. One-way ANOVA with a Tukey's multiple comparison comparing the mean of changes in formation of rosettes. RhoGEF2 vs. RhoGAP71E, p= 0.0015. RhoGAP71E vs. RhoGEF2/RhoGAP71E, p = 0.0056. RhoGEF2 vs. RhoGEF2/RhoGAP71E, p= 0.3789, N= 80-100 edges.

SUPPLEMENTAL MOVIES

Movie 1: Medioapical F-actin network dynamics in WT LCs. (Corresponds to Fig. 1). Time-lapse videos of F-actin (Utr::GFP) in WT that highlight medioapical actomyosin dynamics. Left panel: yellow arrowheads show the fusion of two F-actin nodes in the 2° LC demarcated by the white box. Right panel: red arrow shows the formation of a medioapical ring-like structure, the subsequent disassembly of the ring and flow of actin to the LC-LC contact (note the green arrow movement).

Movie 2: Medioapical actomyosin network ablation induces asymmetric cell expansion of the 2° and 3° LCs. (Correspond to Fig. 2). Time-lapse videos of a 2° (left panel) and a 3° (right panel) LCs that express F-actin (Utr::GFP) and MyoII (MyoII::mCh). Targeted ablations of the medioapical actomyosin network in the LCs induced a rapid asymmetric apical cell area relaxation (note the area of the 2° and 3° LCs highlighted by the white box before and after ablation).

Movie 3: Rho1 expression accelerates medioapical F-actin dynamics in LCs. (Corresponds to Fig. 3). Time-lapse videos of F-actin (Utr::GFP) dynamics in WT retina (left panel) and in a retina that expresses

Rho1 (right panel). Note the robust and accelerated assembly and disassembly of medioapical F-actin in the LCs in the retina that expresses Rho1. This faster turnover of the medioapical actomyosin network led to a rapid decrease and increase in the apical cell area. Red and green arrowheads highlight the assembly and disassembly of the medioapical actomyosin network, respectively.

Movie 4: The medioapical actomyosin network assembles and dissembles in response to mechanical inputs. (Corresponds to Fig. 3). Time-lapse video of a fly retina that express Rho1 compared with WT. Rho1 expression accelerated the assembly and disassembly of the medioapical F-actin networks and cell area contraction and expansion. Note that this behavior is inversely coordinated between the two adjacent 2° LCs demarcated by the white box. Green arrowhead marks medioapical F-actin assembly; red arrowhead marks disassembly.

Movie 5: Constitutive F-actin and MyoII assembly disrupts medioapical actomyosin organization and dynamics. (Corresponds to Fig.4). (Left) Time-lapse video of MyoII (MyoII::mCh) in $MLCK^{CA}$ eyes that activate MyoII. Note the rapid assembly and disassembly of a medioapical ring marked with yellow arrowheads. (Right) A time-lapse video of F-actin (Utr::GFP) in Dia^{CA} eyes that activate the assembly of linear actin filaments. Note the increased F-actin levels around the LCs' borders and the low levels and dynamics of medioapical F-actin.

Movie 6: RhoGEF2 accelerates medioapical F-actin and MyoII dynamics in LCs. (Correspond to Fig. 5) Left: A time-lapse video of F-actin (Utr::GFP) in eyes that overexpress RhoGEF2. Note the rapid assembly and disassembly of the medioapical F-actin network marked by the red and green arrowheads, respectively. Middle and right: A time-lapse video of MyoII (MyoII::mCh) in cell clones that express a RhoGEF2 RNAi (GFP^{+}, white arrowhead) compared with WT counterpart (yellow arrowhead). Right: Note loss of MyoII intensity in the RhoGEF2 RNAi expressing 2° LC compared with the WT.

Movie 7: RhoGAP71E inhibits medioapical F-actin and MyoII dynamics in LCs. (Correspond to Fig. 6) Left: Time-lapse video of F-actin (Utr::GFP) in eyes that overexpress RhoGAP71E. Note the increased apical cell area of the LCs and reduced medioapical F-actin levels. Middle: Time-lapse video of MyoII (MyoII::mCh) in clones expressing RhoGAP71E RNAi, positively marked with RFP. Right: Note the reduced apical cell area of the RhoGAP71E RNAi expressing cell (white arrowhead) compared with WT (yellow arrowhead).

Figure 1

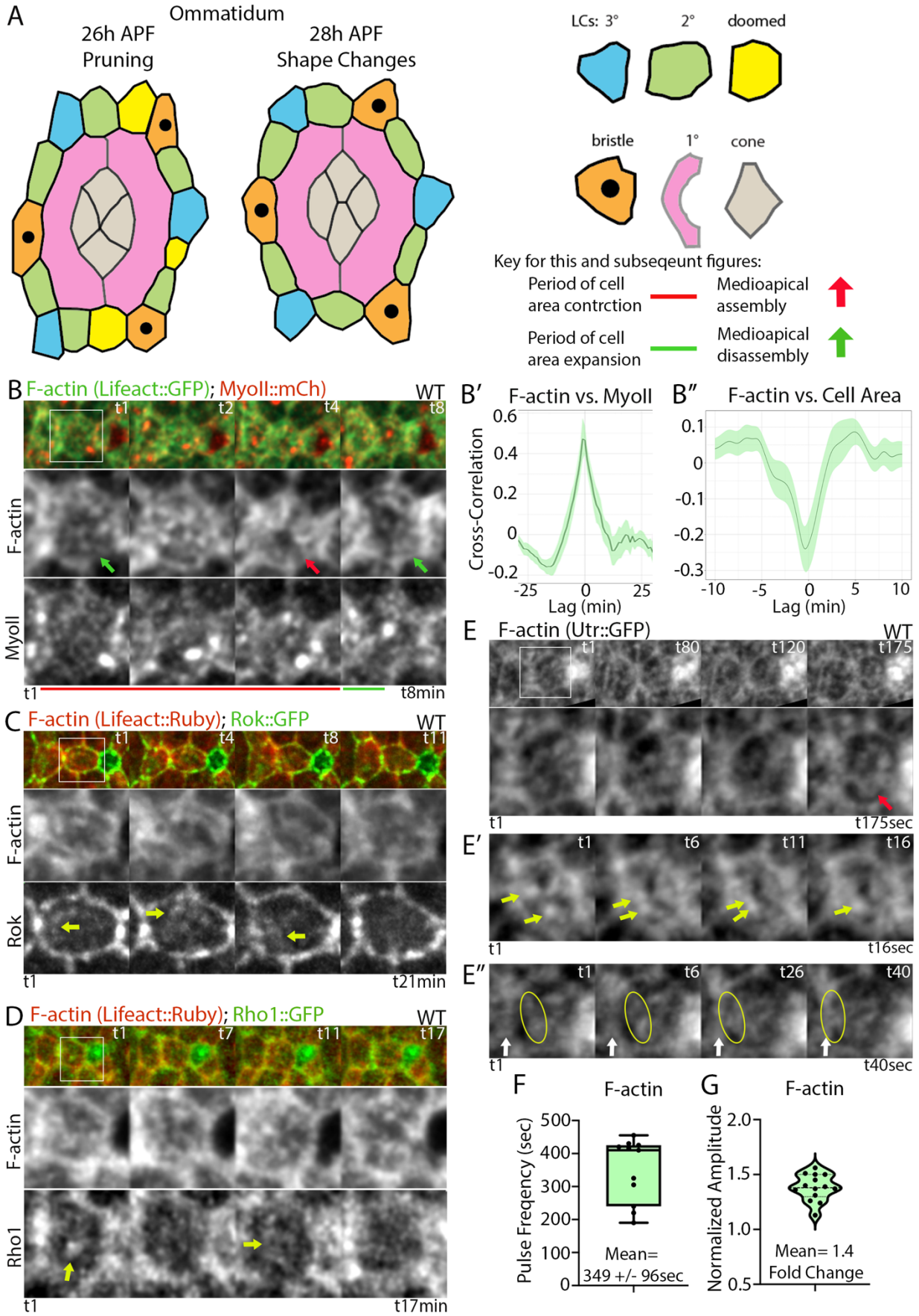
A
Ommatidum
26h APF
Pruning
28h APF
Shape Changes
LCs: 3°
2°
doomed
bristle
1°
cone
Key for this and subseqeunt figures:
Period of cell area contrction
Medioapical assembly
Period of cell area expansion
Medioapical disassembly
B F-actin (Lifeact::GFP); MyoII::mCh)
WT
t1
t2
t4
t8
F-actin
MyoII
t8min
B′ F-actin vs. MyoII
B″ F-actin vs. Cell Area
Cross-Correlation
Lag (min)
C F-actin (Lifeact::Ruby); Rok::GFP
t11
Rok
t21min
D F-actin (Lifeact::Ruby); Rho1::GFP
t7
t17
Rho1
t17min
E F-actin (Utr::GFP)
t80
t120
t175
t175sec
E′
t6
t16
t16sec
E″
t26
t40
t40sec
F F-actin
Pulse Freqency (sec)
Mean=
349 +/- 96sec
G F-actin
Normalized Amplitude
Mean= 1.4
Fold Change

Figure 2

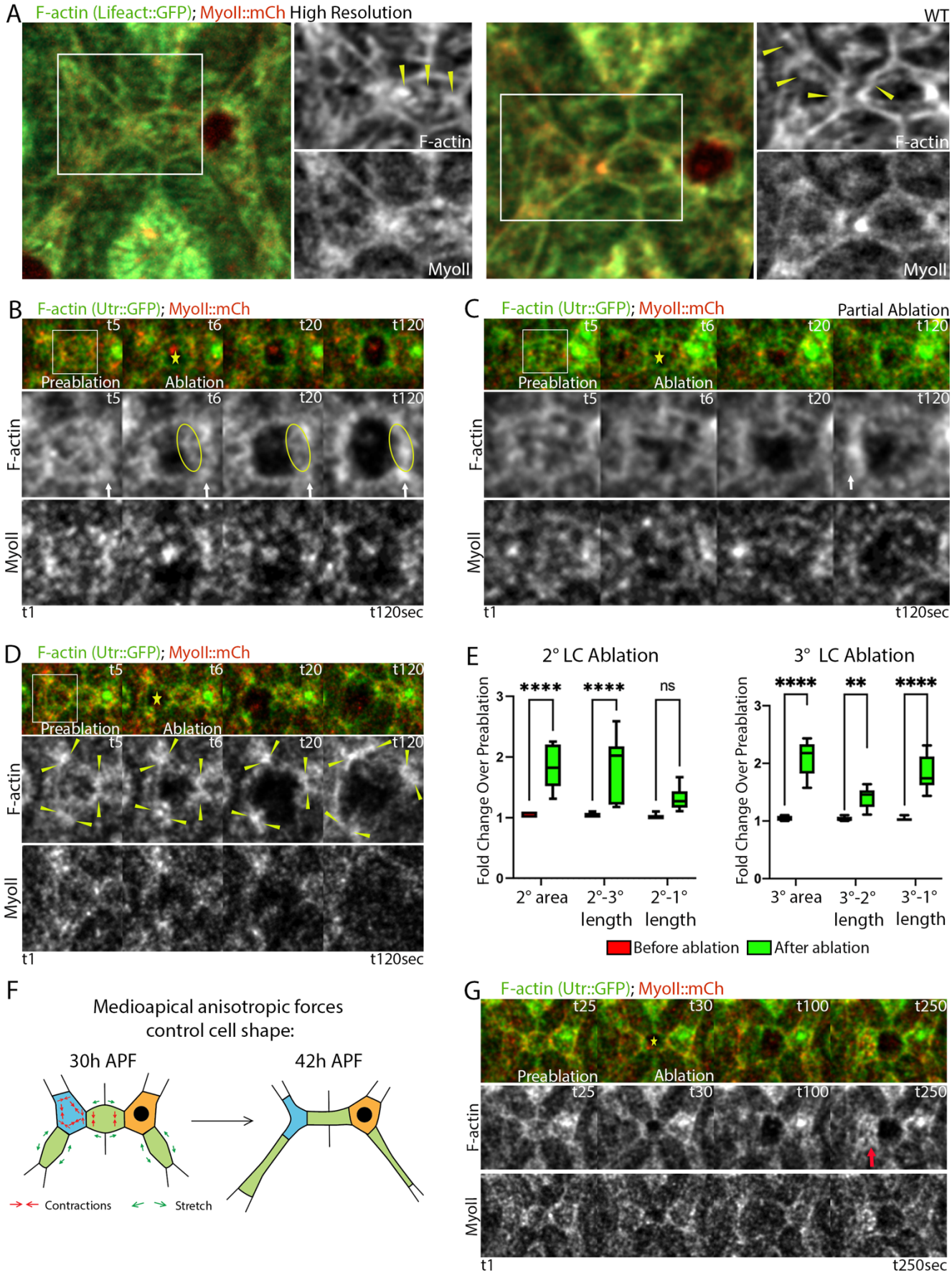
A
F-actin (Lifeact::GFP); MyoII::mCh High Resolution
WT
F-actin
MyoII
B
F-actin (Utr::GFP); MyoII::mCh
t5
t6
t20
t120
Preablation
Ablation
F-actin
MyoII
t1
t120sec
C
F-actin (Utr::GFP); MyoII::mCh
Partial Ablation
D
E
2° LC Ablation
3° LC Ablation
Fold Change Over Preablation
****
ns
**
2° area
2°-3° length
2°-1° length
3° area
3°-2° length
3°-1° length
Before ablation
After ablation
F
Medioapical anisotropic forces control cell shape:
30h APF
42h APF
Contractions
Stretch
G
F-actin (Utr::GFP); MyoII::mCh
t25
t30
t100
t250
t250sec

Figure 3

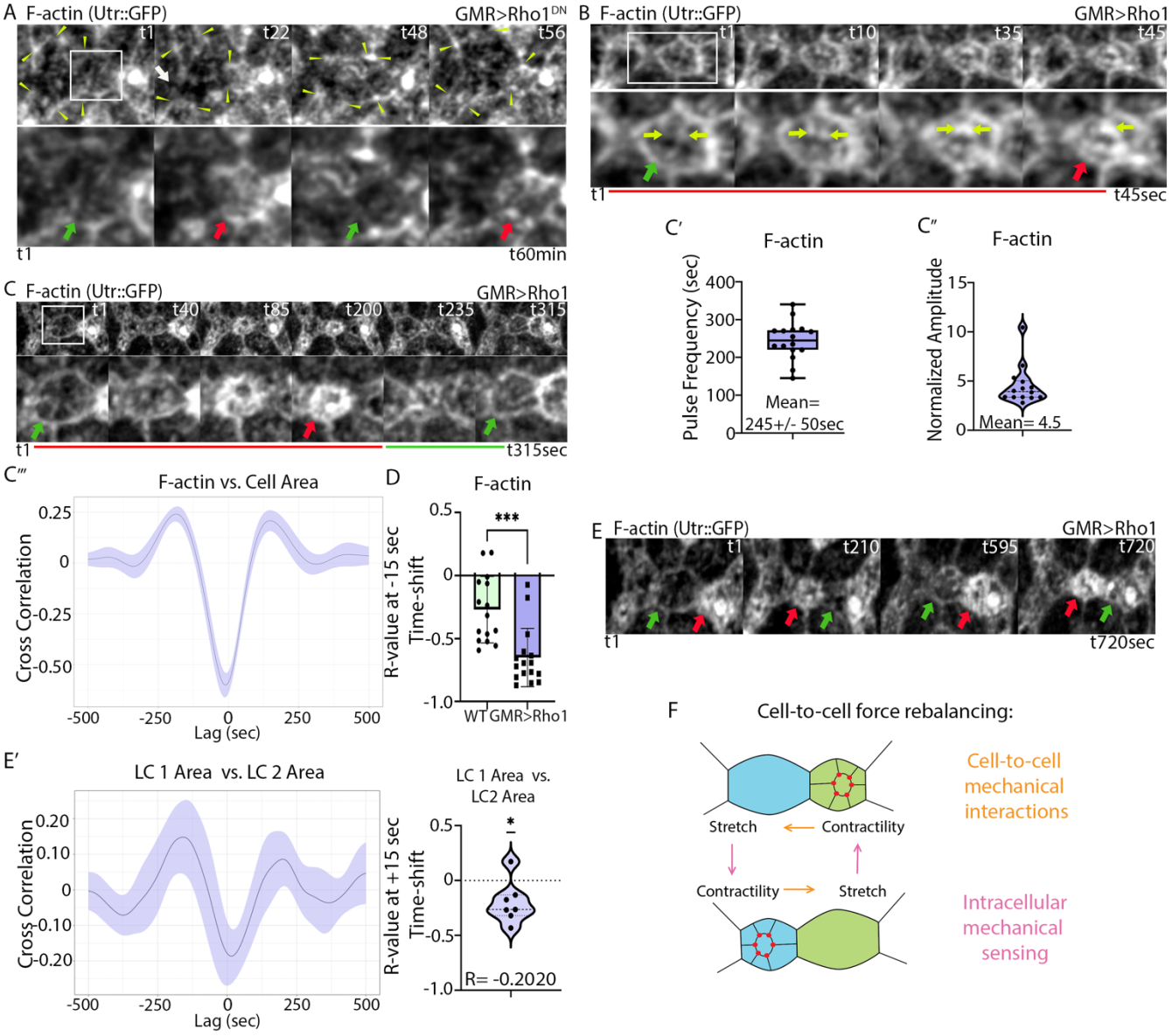
A F-actin (Utr::GFP)
GMR>Rho1DN
t1
t22
t48
t56
t60min
B F-actin (Utr::GFP)
GMR>Rho1
t1
t10
t35
t45
t45sec
C F-actin (Utr::GFP)
GMR>Rho1
t1
t40
t85
t200
t235
t315
t315sec
C′
F-actin
Pulse Frequency (sec)
Mean=
245+/- 50sec
C″
F-actin
Normalized Amplitude
Mean= 4.5
C‴
F-actin vs. Cell Area
Cross Correlation
Lag (sec)
D
F-actin
R-value at -15 sec
Time-shift
***
WT
GMR>Rho1
E F-actin (Utr::GFP)
GMR>Rho1
t1
t210
t595
t720
t720sec
E′
LC 1 Area vs. LC 2 Area
Cross Correlation
Lag (sec)
LC 1 Area vs.
LC2 Area
R-value at +15 sec
Time-shift
*
R= -0.2020
F
Cell-to-cell force rebalancing:
Stretch
Contractility
Contractility
Stretch
Cell-to-cell
mechanical
interactions
Intracellular
mechanical
sensing

Figure 4

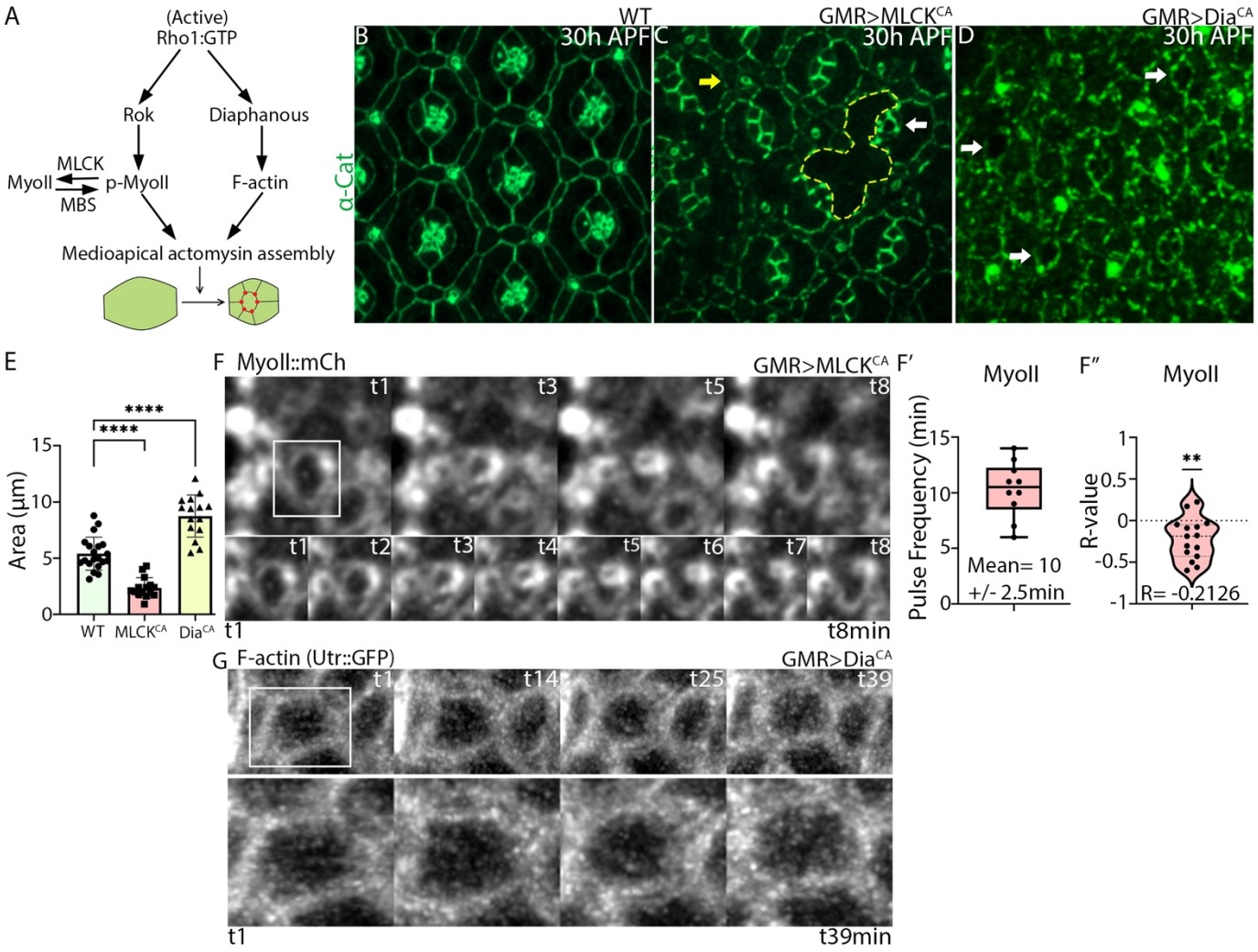
A
(Active)
Rho1:GTP
Rok
Diaphanous
MLCK
MyoII
p-MyoII
MBS
F-actin
Medioapical actomysin assembly
WT
GMR>MLCK^CA
GMR>Dia^CA
B
30h APF
C
30h APF
D
30h APF
α-Cat
E
Area (µm)
****
****
WT
MLCK^CA
Dia^CA
F MyoII::mCh
GMR>MLCK^CA
t1
t3
t5
t8
t1
t2
t3
t4
t5
t6
t7
t8
t1
t8min
F′
MyoII
Pulse Frequency (min)
Mean= 10
+/- 2.5min
F″
MyoII
R-value
**
R= -0.2126
G F-actin (Utr::GFP)
GMR>Dia^CA
t1
t14
t25
t39
t1
t39min

Figure 5

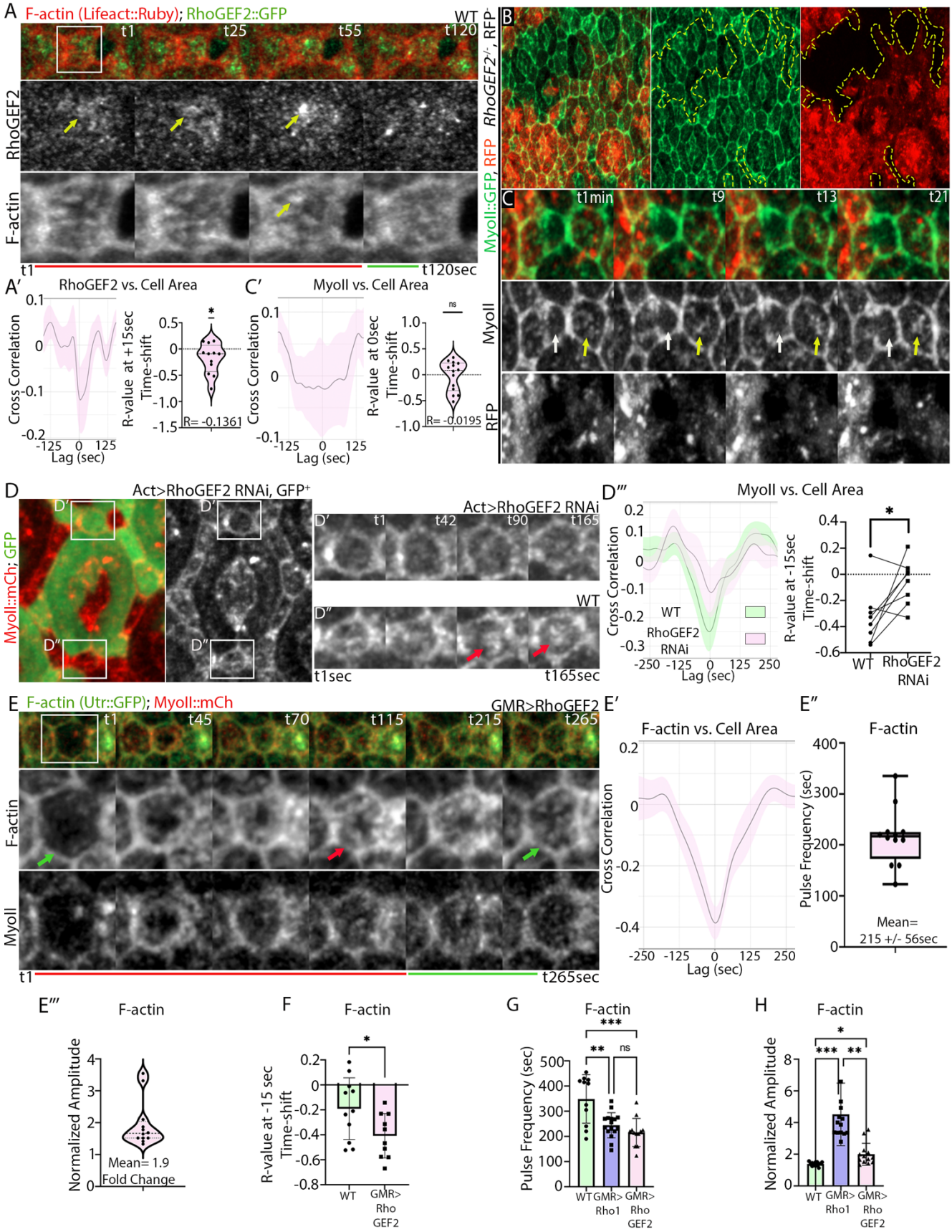
A
F-actin (Lifeact::Ruby); RhoGEF2::GFP
WT
t1
t25
t55
t120
RhoGEF2
F-actin
t120sec
A′
RhoGEF2 vs. Cell Area
Cross Correlation
Lag (sec)
R-value at +15sec
Time-shift
R= -0.1361
C′
MyoII vs. Cell Area
R-value at 0sec
R= -0.0195
B
RhoGEF2-/-, RFP
MyoII::GFP, RFP
C
t1min
t9
t13
t21
MyoII
RFP
D
Act>RhoGEF2 RNAi, GFP+
MyoII::mCh; GFP
D′
D″
Act>RhoGEF2 RNAi
t42
t90
t165
WT
t1sec
t165sec
D‴
MyoII vs. Cell Area
RhoGEF2 RNAi
R-value at -15sec
E
F-actin (Utr::GFP); MyoII::mCh
GMR>RhoGEF2
t45
t70
t115
t215
t265
t265sec
E′
F-actin vs. Cell Area
E″
F-actin
Pulse Frequency (sec)
Mean=
215 +/- 56sec
E‴
Normalized Amplitude
Mean= 1.9
Fold Change
F
R-value at -15 sec
GMR>
Rho
GEF2
G
H
Rho1

Figure 6

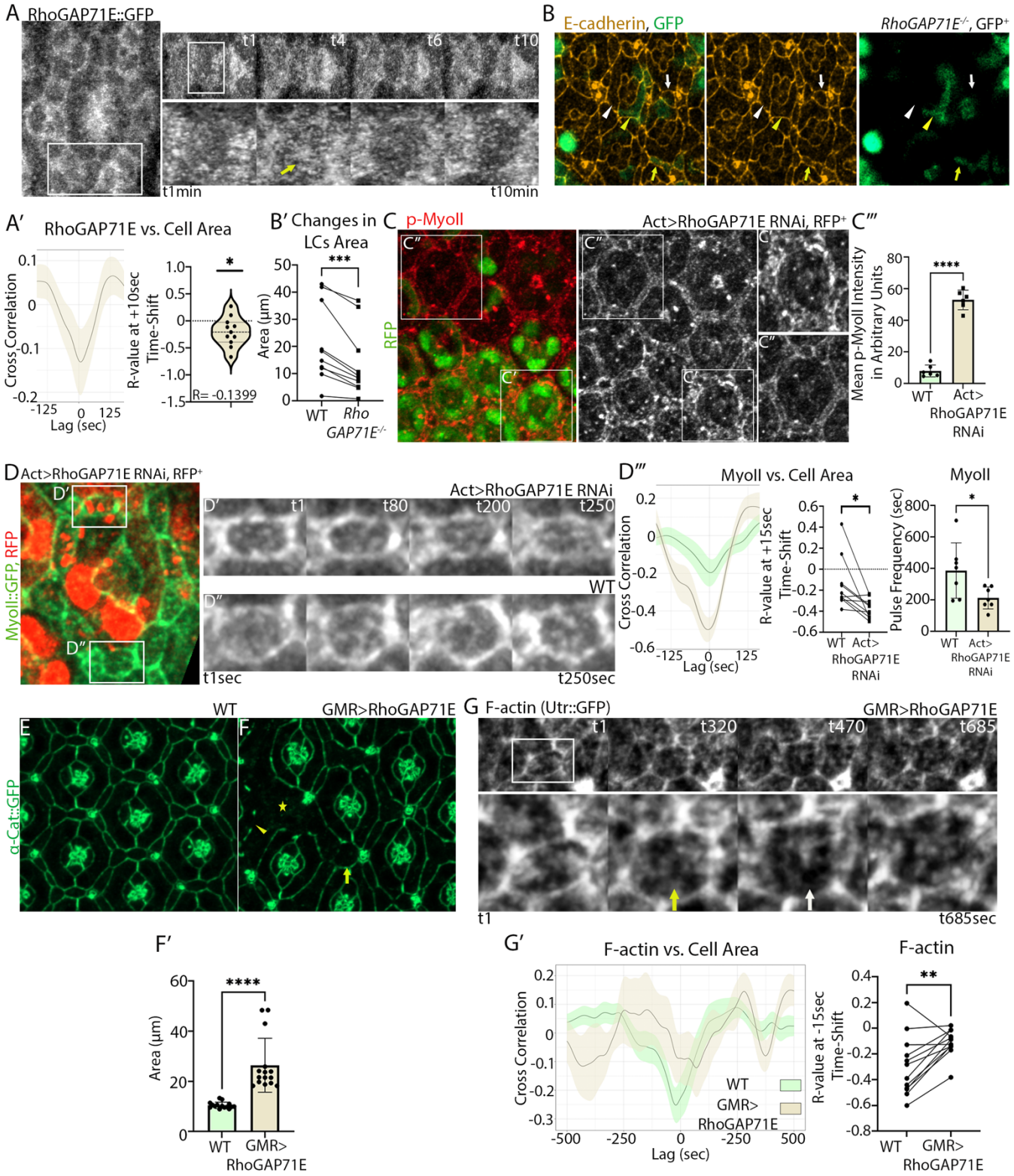
A RhoGAP71E::GFP
t1
t4
t6
t10
t1min
t10min
B E-cadherin, GFP
RhoGAP71E-/-, GFP+
A′ RhoGAP71E vs. Cell Area
Cross Correlation
Lag (sec)
R-value at +10sec Time-Shift
R= -0.1399
B′ Changes in LCs Area
Area (µm)
WT
Rho GAP71E-/-
C p-MyoII
RFP
Act>RhoGAP71E RNAi, RFP+
C‴
Mean p-MyoII Intensity in Arbitrary Units
WT
Act> RhoGAP71E RNAi
D Act>RhoGAP71E RNAi, RFP+
MyoII::GFP, RFP
Act>RhoGAP71E RNAi
WT
t1sec
t250sec
D‴ MyoII vs. Cell Area
Cross Correlation
Lag (sec)
R-value at +15sec Time-Shift
MyoII
Pulse Frequency (sec)
WT
Act> RhoGAP71E RNAi
WT
GMR>RhoGAP71E
α-Cat::GFP
G F-actin (Utr::GFP)
GMR>RhoGAP71E
t1
t320
t470
t685
t685sec
F′
Area (µm)
WT
GMR> RhoGAP71E
G′ F-actin vs. Cell Area
Cross Correlation
Lag (sec)
WT
GMR> RhoGAP71E
R-value at -15sec Time-Shift
F-actin

Figure 7

Rho1-dependent regulation of cellular force balance:

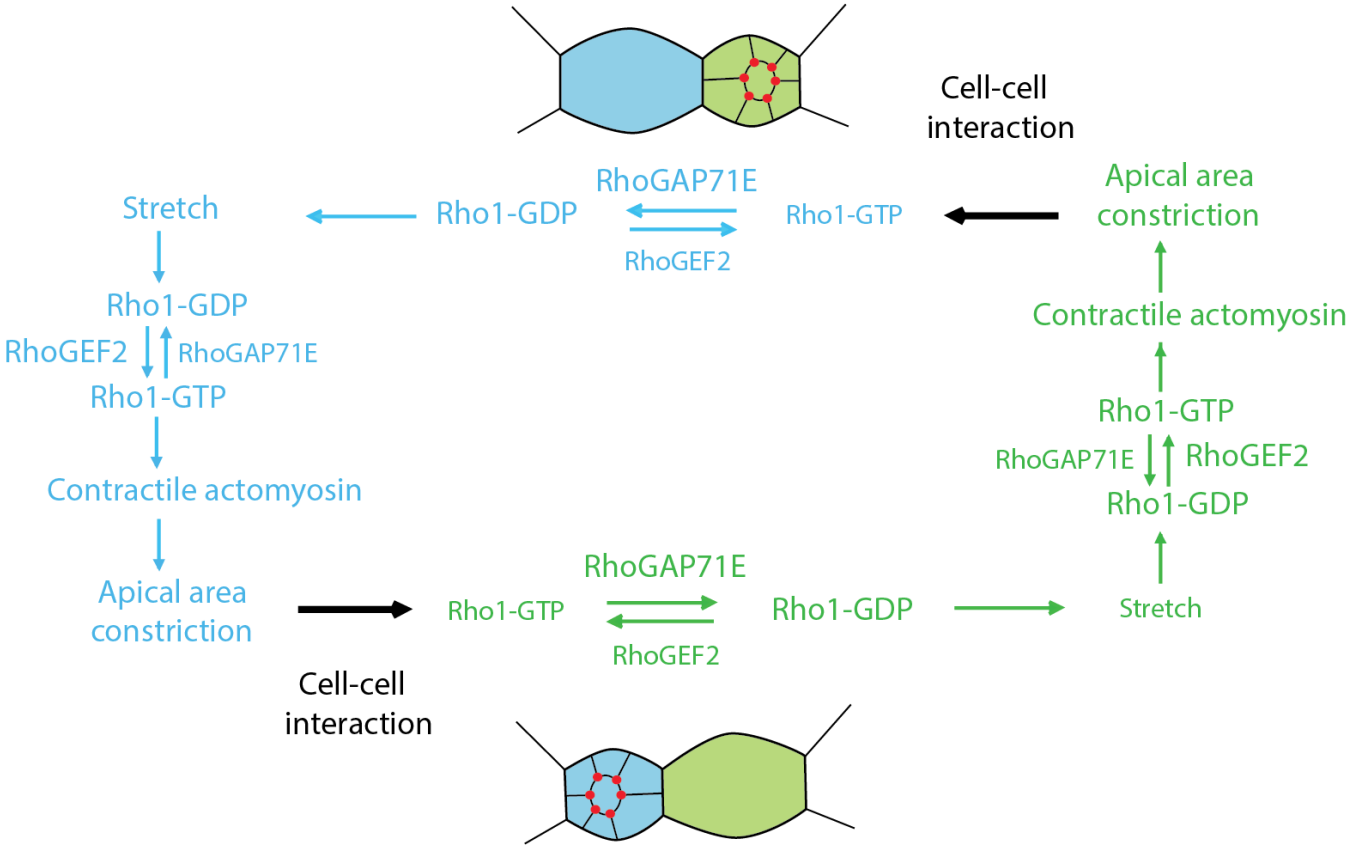

Figure S1

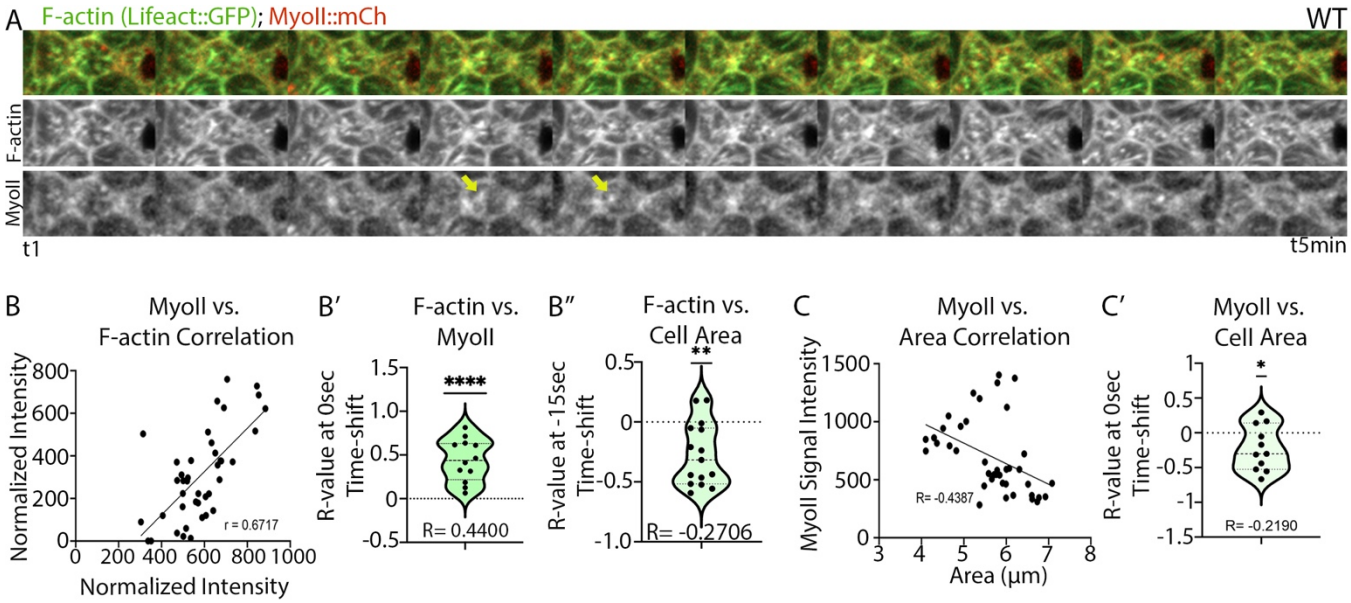
A
F-actin (Lifeact::GFP); MyoII::mCh
WT
F-actin
MyoII
t1
t5min
B
MyoII vs.
F-actin Correlation
Normalized Intensity
r = 0.6717
Normalized Intensity
B′
F-actin vs.
MyoII
R-value at 0sec
Time-shift
****
R= 0.4400
B″
F-actin vs.
Cell Area
R-value at -15sec
Time-shift
**
R= -0.2706
C
MyoII vs.
Area Correlation
MyoII Signal Intensity
R= -0.4387
Area (µm)
C′
MyoII vs.
Cell Area
R-value at 0sec
Time-shift
*
R= -0.2190

Figure S2

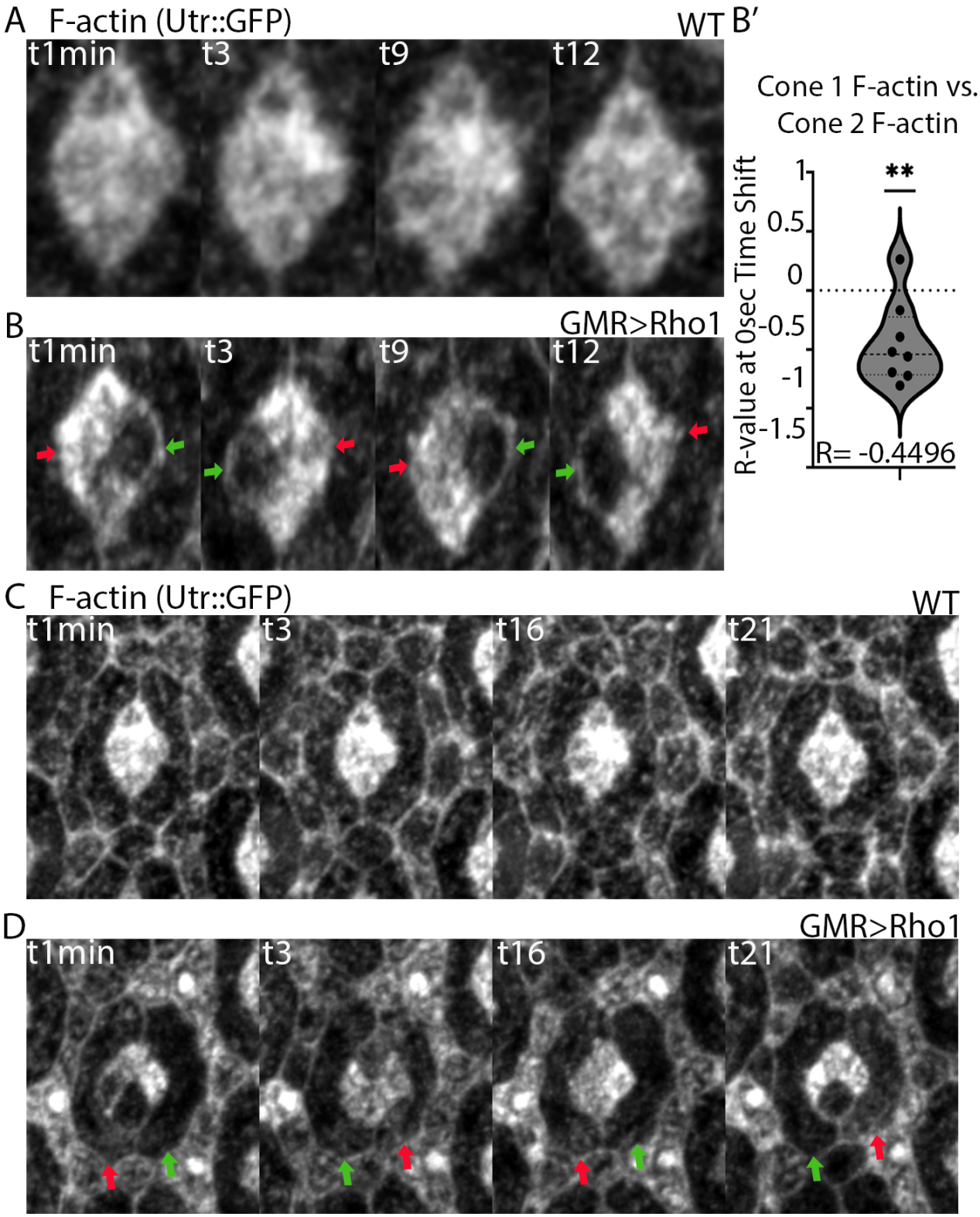
A F-actin (Utr::GFP)
WT
t1min
t3
t9
t12
B
GMR>Rho1
t1min
t3
t9
t12
B′
Cone 1 F-actin vs.
Cone 2 F-actin
R-value at 0sec Time Shift
1
0.5
0
-0.5
-1
-1.5
**
R= -0.4496
C F-actin (Utr::GFP)
WT
t1min
t3
t16
t21
D
GMR>Rho1
t1min
t3
t16
t21

Figure S3

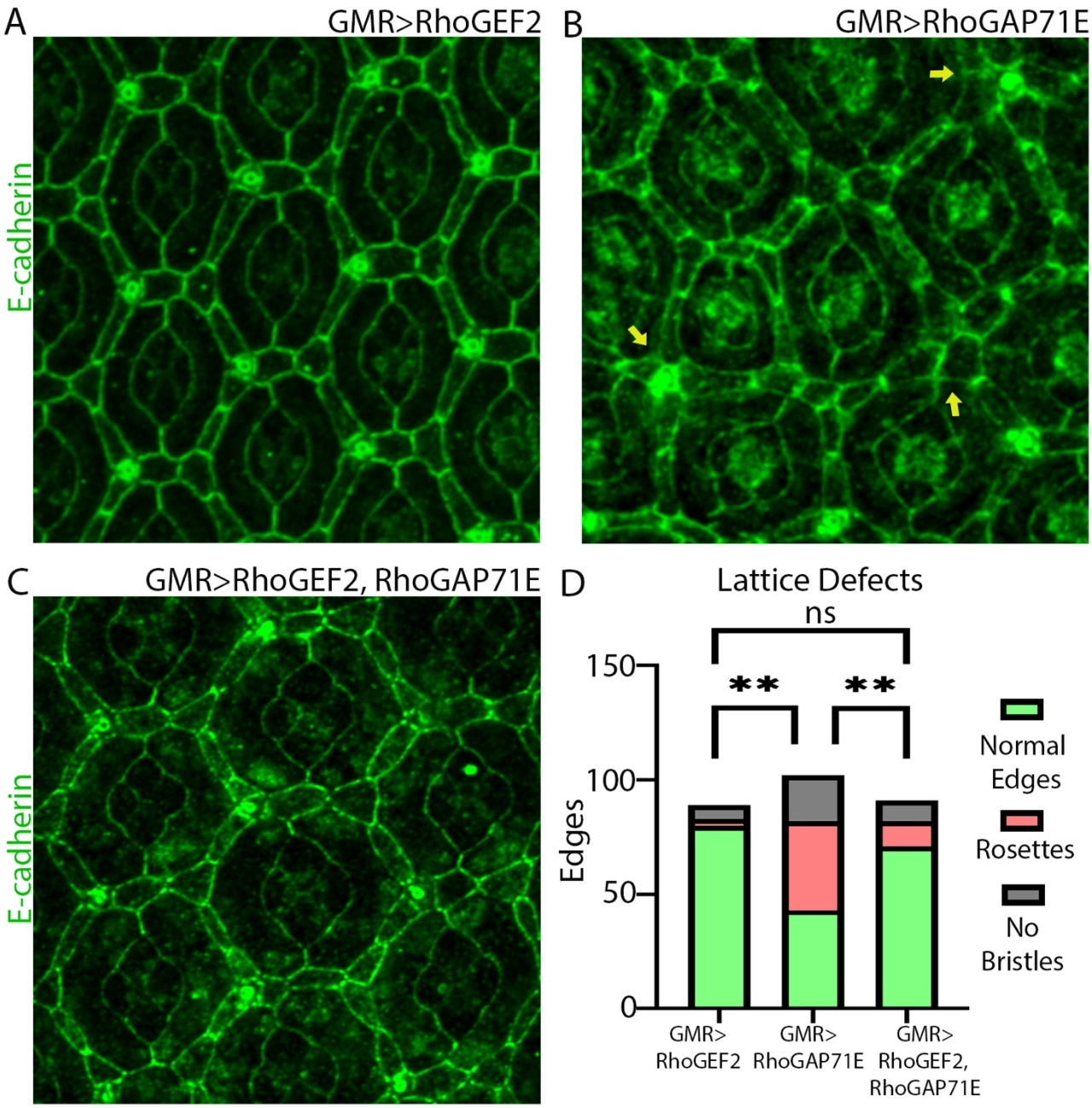
A
GMR>RhoGEF2
E-cadherin
B
GMR>RhoGAP71E
C
GMR>RhoGEF2, RhoGAP71E
E-cadherin
D
Lattice Defects
ns
**
**
150
100
50
0
Edges
Normal Edges
Rosettes
No Bristles
GMR> RhoGEF2
GMR> RhoGAP71E
GMR> RhoGEF2, RhoGAP71E